ANALISIS DE LOS REQUISITOS EXPERIMENTALES NECESARIOS PARA REALIZAR ESTUDIOS DE ESPECTROSCOPIA GAMMA EN VUELO A ENERGIAS RELATIVISTAS

Jose Fernández Vázquez

March 13, 2002

Contents

Introducción

La espectroscopía γ es el estudio de los fotones de alta energía (normalmente del orden de unos keV o MeV) emitidos por fuentes radiactivas como consecuencia de la transición de los núcleos emisores de un estado de más a otro de menos energía. Este estudio de hace con el objetivo de obtener información sobre los distintos niveles energéticos nucleares, como pueden ser espines y paridades, energías, probabilidades de transición, y otros (ver referencias de [1]).

Esta técnica ha sido ampliamente utilizada en los últimos 50 años [2]. Tradicionalmente, los rayos γ eran detectados una vez que el núcleo estaba parado o bien se movía a muy baja energía.

Hoy en día, con la disponibilidad de los Haces Nucleares Radiactivos (RNB en inglés) [3], la física nuclear ha desplazado su interés hacia la parte más exótica de la tabla de núcleos.

El estudio de esas nuevas especies exóticas brinda un nuevo contexto experimental y las técnicas existentes han de ser revisadas (y/o modificadas) para mantener su utilidad.

En el caso particular de la espectroscopía de rayos γ, las cortas vidas de esos núcleos tan exóticos representan un problema para la aplicación de la técnica "tradicional". El tiempo necesario para producir, identificar y detener al núcleo de interés es demasiado largo comparado con su vida media.

Entre las soluciones propuestas, el estudio de núcleos exóticos en estados isoméricos (con vidas medias muy largas) representa una posibilidad realmente elegante [4].

Otra forma de atacar el problema es producir los núcleos exóticos en una facilidad "en vuelo", por medio de la fragmentación (o fisión) de los

núcleos de un haz primario, para identificarlos "en vuelo" con la ayuda de espectrómetros magnéticos.

Para producir dichos núcleos de un modo eficiente, el proceso ha de realizarse a altas energías (por encima de los 50 MeV/nucleón) y así aprovechar que la distribución angular de los fragmentos saldrá fuertemente picada hacia adelante. De este modo se minimizan las pérdidas por transmisión en el espectrómetro.

Por otra parte, las elevadas velocidades con que se mueven los fragmentos nos permiten identificarlos muy rápidamente (a mayor velocidad, menos tiempo se necesita).

Esto nos ofrece la posibilidad de estudiar un gran número de núcleos exóticos de vida media corta, si al mismo tiempo detectamos los rayos γ emitidos por esos fragmentos.

Esta técnica recibe el nombre de: espectroscopía de rayos γ (emitidos) "en vuelo".

La espectroscopía gamma en vuelo es una herramienta muy útil para explorar las zonas más exóticas de la tabla de núcleos. El rango energético "clásico" para esta técnica estuvo en un principio restringido a energías alrededor de la barrera Coulombiana [5], pero experimentos recientes han extendido el límite hasta valores de 90-100 MeV/nucleón [6, 7].

Esta limitación se debía fundamentalmente a las dificultades cinemáticas que se hallaban a altas energías. La identificación de rayos gamma emitidos por una fuente en movimiento sufre de dos efectos:

- El corrimiento Doppler: La radiación emitida por una fuente en movimiento se observa con una energía o frecuencia distinta. Esto se conoce como efecto Doppler y su primera consecuencia es un corrimiento en las energías de los gammas observados en los detectores. Es posible corregir el corrimiento Doppler usando la ecuación 1. Para llevar a cabo esta corrección debemos conocer la trayectoria del emisor. Sin embargo, esta corrección presenta ciertas limitaciones que serán discutidas más adelante.

2

$$E = E_{lab} \cdot \frac{1 - \beta \ cos \ \theta_{lab}}{\sqrt{1 - \beta^2}} \tag{1}$$

La fórmula anterior permite obtener la energía del rayo γ en el sistema de referencia del emisor (E), como función de la energía del gamma en el sistema de referencia del laboratorio (E_{lab}), de la velocidad del emisor con respecto al detector (β), y del ángulo de emisión del rayo γ con respecto a la dirección del emisor en el sistema de referencia del laboratorio (θ_{lab}).

- El ensanchamiento Doppler: Se debe parcialmente a la incertidumbre angular introducida por nuestros detectores de rayos γ, y puede ser entendida del siguiente modo. Cuando un rayo γ es emitido, sufre un corrimiento Doppler que depende del ángulo que forma con la traza de la fuente. Si conociésemos este ángulo con total precisión, podríamos hacer una corrección Doppler para obtener la energía del rayo γ en el sistema de referencia del emisor. Para obtener esta información angular se emplea la posición del detector golpeado por el rayo γ. Pero un detector no es un dispositivo puntual, tiene un cierto volumen. Experimentalmente sólo podemos asignar una única posición angular por detector y es por ello que se obtiene una dispersión en la señal después de la corrección Doppler. Este efecto es mayor para mayores velocidades de la fuente. Desafortunadamente, no puede ser eliminado.

De acuerdo con la ecuación 1, cuanto mayor sea la velocidad del emisor, mayor es la energía observada para el rayo γ. En consecuencia, necesitamos detectores de rayos γ con una buena respuesta en eficiencia para altas energías.

El objetivo de este trabajo es el estudio de las condiciones experimentales particulares que nos encontramos cuando queremos aplicar la técnica de la espectroscopía γ en vuelo a energías relativistas, así como la definición de un dispositivo experimental que se adecúe a la detección de rayos gamma bajo estas condiciones cinemáticas particulares.
Para ello realizamos un experimento en el GSI en el que se estudió la detección de rayos γ en vuelo. Dichos rayos γ procedían de la desexcitación de residuos de reacciones de rotura con proyectiles exóticos a energías relativistas. Como se trabaja a energías alrededor de 1 GeV/nucleón, que son velocidades extremadamente altas para la espectroscopía γ tradicional, el efecto Doppler es especialmente importante. De hecho, a esas energías (β=0.8667c)

la resolución que tenemos (en energías) está limitada por el ensanchamiento Doppler. Todo esto provocó que escogiéramos detectores de NaI dispuestos en un array que cubría un ángulo sólido máximo hacia adelante, dejando al mismo tiempo espacio para que pasara el haz.

Era imposible realizar experimentalmente una calibración en eficiencia a las energías esperadas para gammas procedentes de fuentes en movimiento a energías relativistas, porque no disponíamos de ninguna fuente que emitiera rayos γ con una energía tan alta. Además, la distribución angular de la emisión de gammas por parte de una fuente en movimiento es totalmente distinta de la de la emisión por parte de la misma fuente en reposo. Por esta razón, se necesitaba una simulación completa del detector de rayos γ para obtener esa información. Al mismo tiempo, era necesaria una calibración precisa en eficiencias para rayos γ de hasta 3 MeV (emitidos en reposo) para comprobar la calidad de la simulación.

En primer lugar se presenta el experimento que se llevó a cabo, junto con información técnica como son las características del haz y los detectores empleados. Esto se hace en el capítulo 1.

Después de esta introducción general del montaje experimental, en el capítulo 2 la atención se centra en el detector de rayos γ (el array de cristales de NaI) y se explica cómo se han hecho las diferentes calibraciones en tiempo, energía, resolución en energía y eficiencia total.

En el capítulo 3 se presenta la simulación realizada para el array de cristales de NaI y los resultados obtenidos son comparados con las medidas reales cuando esto es posible.

La simulación es también una herramienta muy poderosa para analizar diferentes geometrías, y/o detectores que podrían mejorar la eficiencia de detección de rayos γ para futuros experimentos, como se muestra en el capítulo 4.

Finalmente se expone la conclusión a todo este trabajo.

Introduction

Gamma ray spectroscopy is the study of the high energy photons (usually around keV or MeV) emitted by radioactive sources due to the transition of the emitter nuclei between different states (from higher to lower energy). The reason for doing γ ray spectroscopy is to obtain information about the different energetic nuclear levels, like spin and parity, energy, transition probability, and other characteristics (see references of [1]).

This technique has been widely used in the last 50 years [2]. Traditionally, the De-excitation γ rays were detected once the nucleus was stopped or moving with a very low energy.

Nowadays, with the availability of Radioactive Nuclear Beams (RNB) [3], nuclear physics has moved its interest to the very exotic part of the nuclei chart.

The study of those new exotic species brings a new experimental context and the existing techniques have to be revised (and/or modified) in order to keep their capabilities.

In the particular case of the γ ray spectroscopy, the short life times of these very exotic nuclei represents a problem for the application of the "traditional" technique. The time necessary to produce, identify and stop the interesting nucleus is too long compared to its life time.

Among the solutions proposed, the study of exotic nuclei in isomeric states (with very long life times) represents a very elegant possibility [4].

Another way to overcome this problem is to produce the exotic nuclei in an "in-flight" facility from primary beam fragmentation (or fission) and to identify them "in-flight" with the help of magnetic spectrometers.

In order to produce efficiently those exotic nuclei, the process has to take place at high energies (over 50 MeV/nucleon) to take profit of the peaked forward angular distribution of the fragments. In this way we minimize the transmission loses in the spectrometer.

In another hand, the high velocities allow us to identify the fragments in a very short time (shorter for higher velocities).

This gives us the possibility to study a large number of short lived exotic nuclei, if at the same time we detect the γ rays emitted by those fragments.

This technique is called: "in-beam" γ ray spectroscopy.

In-beam gamma ray spectroscopy is a very useful tool to explore the exotic area of the chart of the nuclides. The "classical" energetic range for this technique was initially restricted to energies around the Coulomb barrier [5], but recent experiments have extended the limit to values of 90-100 MeV/nucleon [6, 7].

This limitation came basically by the kinematic difficulties encountered at high energies. The identification of gamma rays emitted from a moving source suffers from two effects:

- The Doppler shift: The radiation emitted from a moving source is observed with a different frequency or energy. This is known as Doppler effect and its first consequence is a shift in the energies of the γ rays observed at the detectors. It is possible to correct the Doppler shift using the equation 2. To perform this correction we should know the trajectory of the emitter. However, this correction presents certain limitations that will be discussed below.

$$E = E_{lab} \cdot \frac{1 - \beta \ cos \ \theta_{lab}}{\sqrt{1 - \beta^2}} \tag{2}$$

  The above formula gives the energy of the γ ray in the emitter reference system (E), as a function of the energy of the gamma in the laboratory reference system (E_{lab}), the velocity of the emitter related to the detector (β), and the emission angle of the γ ray with respect to the direction of the emitter in the laboratory reference system (θ_{lab}).

- The Doppler broadening: It is partially due to the angular uncertainty introduced by our γ detectors, and it can be understood in the following way. When a γ ray is emitted, it suffers a Doppler shift that depends on the angle it forms with the source track. If we knew this angle with total precision, we could do a Doppler correction to get the energy of the γ ray at the emitter reference system. To obtain this angular information, we use the position of the detector hit by the γ ray. But a detector is not a punctual device, it has a certain volume. Experimentally we can only assign a unique angular position per detector and then a smearing in the signal after the Doppler correction is obtained. This effect is higher for higher source velocities. Unfortunately, it cannot be eliminated.

According to equation 2, the higher the velocity of the emitter is, the higher the energy observed for the γ ray results. Consequently, we need γ ray detectors with good efficiency response at high energies.

The goal of this work is the study of the particular experimental conditions that we find when we want to apply the in-beam γ ray spectroscopy (at relativistic energies) technique and, at the same time, the definition of a experimental device specially devoted to γ rays detection under these kinematic conditions.

To accomplish this, we performed an experiment in the GSI where we studied in-beam γ rays detection. Those gamma rays came from the De-excitation of fragments produced from exotic projectiles in breakup reactions at relativistic energies. Since we are working at energies around 1 GeV/nucleon, which are extremely high velocities for traditional γ spectroscopy, the Doppler effect is specially important. In fact, at these energies (β=0.8667c) our energy resolution is limited by the large Doppler broadening. These considerations convinced us to choose NaI detectors disposed in an array covering a maximum solid angle in the forward direction, leaving at the same time place for the beam to pass through it.

The efficiency calibration at the energies expected for the γ rays coming from a moving source at relativistic energies was impossible to be done experimentally because we did not have any source providing γ rays at so high energy. In addition, the angular distribution of the γ emission is completely different for stopped and moving sources. In this way, we needed a complete simulation of the γ detector to obtain such information. At the same time, a

7

precise efficiency calibration had to be done for γ rays up to 3 MeV emitted at rest in order to check the quality of the simulation.

We present first the experiment that took place, together with technical information such as the beam characteristics and the used detectors. This is done in chapter 1.

After this general introduction of the experimental setup, in chapter 2 we center our attention on the γ ray detector (the NaI crystals array) and we explain how we have done the different time, energy, energy resolution and total efficiency calibrations.

In chapter 3 we present the simulation done for the NaI crystals array geometry and whenever the results obtained can be compared to the real measurements, this is done.

The simulation is also a very powerful tool to analyze different geometries, and/or detectors that could improve the efficiency of γ detection for future experiments as is presented in chapter 4.

Finally, the conclusion to all this work is done.

Chapter 1

The experiment

In this work we will focus on the topic of in-beam γ rays detection, for beam energies around 1 GeV/nucleon. That was only one part in a more complete experiment that took place between July-December 1999 at the Fragment Separator (FRS) in the heavy ion facility (GSI) in Darmstadt, Germany. Before treating specifically the γ spectroscopy subject in the experiment we will give a general overview.

1.1   General description

The goal of the experiment was to obtain precise measurements of the momentum distributions for the very neutron rich nitrogen, oxygen, and fluorine nuclei, distinguishing between the ground state and the possible core excited states contribution. Why? It is known that the momentum distribution of the fragment resulting from a one nucleon breakup reaction is related to the Fourier transform of the wave function for the removed nucleon when it was still part of the parent (the projectile) [11].

The last nucleon wave function is determining the nuclear structure (nuclear radius, shell disposition, ...) of those very nucleon rich nuclei [11, 12, 13]. It is in consequence a very valuable experimental observable to extend our knowledge of nuclear structure to other nuclei far from the stability valley ones.

The production of those very exotic nuclei was done by fragmentation of a stable primary beam (for the moment we can only accelerate stable nuclei) close to the region of the chart of nuclides under exploration.

To produce efficiently these very exotic nuclei, the process had to take place at higher energies. For this reason we needed an accelerator able to provide a relativistic primary beam to optimize the production of the secondary exotic nuclei. In order to separate and identify the produced nuclei, we used a magnetic spectrometer. In our case, as the in-beam γ ray spectroscopy part was combined with the momentum measured from fragments after a one nucleon removal reaction, the spectrometer was used in energy loss mode.

To fulfill this requirements, the experiment was performed at the high resolution magnetic spectrometer FRagment Separator (FRS) [8] at GSI [10] in Darmstadt, Germany (see figure 1.1) .
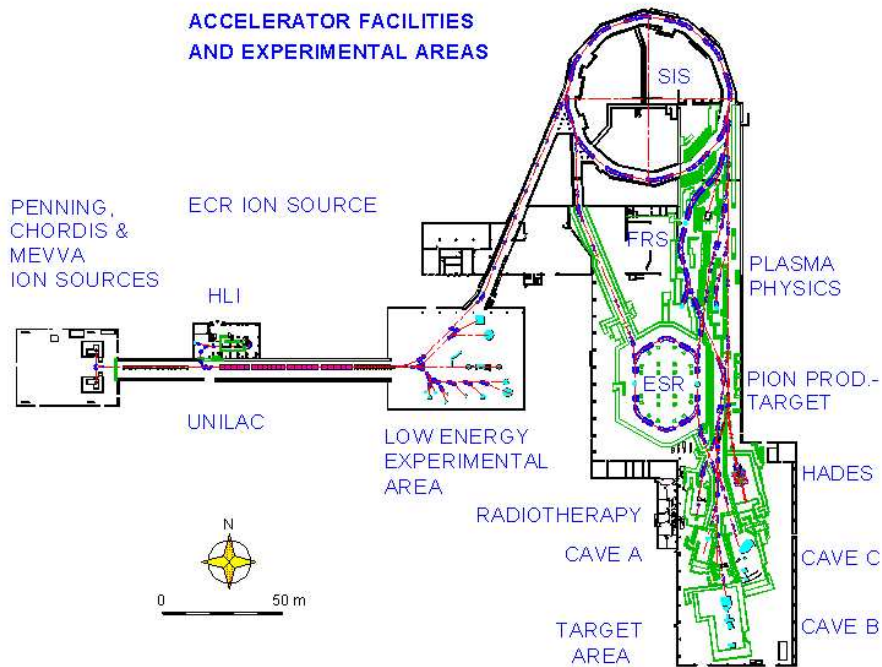

Figure 1.1: *Schematic view of the GSI. Following the beam line, from left to right, and from up to down, we find: the ion sources, the linear accelerator (UNILAC), the low energy experimental area, the synchrotron for heavy ions (SIS), the fragment separator (FRS), the storage ring (ESR), and the high energy experimental area.*

The GSI is a heavy ion research center which is able to provide high energy and high intensity beams, from protons to Uranium, for different applications. It consists mainly in the following areas: the ion sources, the linear accelerator (UNILAC), the low energy experimental area, the synchrotron for heavy ions (SIS), the fragment separator (FRS), the storage ring (ESR), and the high energy experimental area.
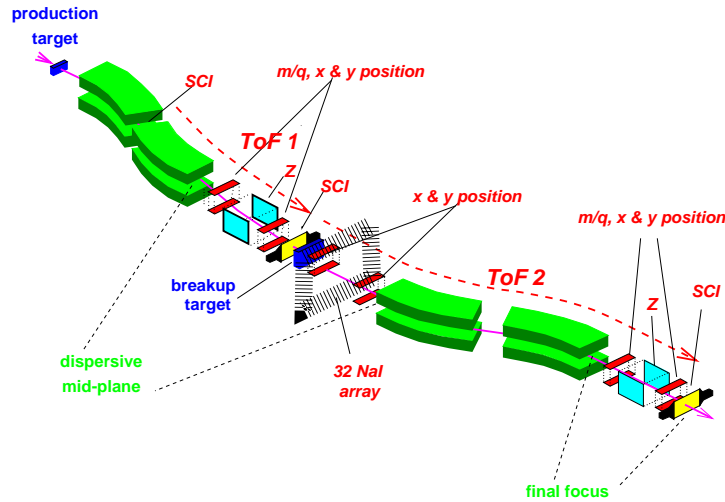

Figure 1.2: *Experimental setup of the FRS used in the experiment (although the FRS is an achromatic magnetic spectrometer, this time it was used in an energy-loss mode, with a target at its central focal plane instead of a degrader [8]. A secondary radioactive beam of projectiles was produced from the primary beam at the production target (on the left). These projectiles loose one or more nucleons after stripping at the intermediate breakup target to give the fragment nuclei. For the complete identification of the projectiles before and after the breakup target, ionization chambers, plastic scintillators and time projection chambers (working as tracking detectors) were used. Finally, gamma rays emitted by the fragments produced in an excited state could be detected by a NaI crystals array.*

In this experiment, a primary beam of ^{40}Ar was produced at the ion sources, and accelerated till around 1 GeV before reaching the production target at the entrance of the FRS. The average primary beam intensity was around 1.5e+10 counts per pulse (for a pulse length of 5 seconds, and 3 seconds between two pulses). At the production target, the ^{40}Ar inpinged over Berilium to produce several products. The first stage magnetic rigidity of the FRS was set to let the $^{20-24}$O pass centered and reach the breakup target

at the middle focal plane of the FRS. Once there, different reactions took place and the fragments $^{19-22}$O were selected to be also centered by the FRS second stage magnetic rigidity (we were interested on one-neutron breakup reactions). It was important to center the nucleus we were interested in to minimize cuts in the emittance due to the limited angular acceptance of the FRS [8] (around ± 0.01 mrad). For specially broad spatial distributions, more than one setting for the magnetic rigidity of the spectrometer was needed in order to cover the complete distribution [11].

To perform in-beam γ ray spectroscopy it is necessary to identify the nuclei (in our case, fragments coming from one nucleon removal reactions) emitting the γ rays. If in addition we are able to identify the projectile before the reaction we have a very powerful selection on the reaction channel. In the experiment, a complete in-flight identification before and after the breakup target was done. We used ionization chambers to determine the charge. Plastic scintillators allowed us to obtain the Time Of Flight (TOF), which means, the nucleus velocity. Time Projection Chambers (TPC's) were used to make the tracking of the particles. Finally, NaI crystal scintillators disposed in an array detected gamma rays coming from excited states of nuclei produced at the breakup target. In figure 1.2 we show a graphical representation of the FRS setup as it was mounted for our experiment.

This γ ray information is in addition very valuable for the complete analysis of the experiment. From the single study of the momentum distributions measured at the end of the spectrometer one can not distinguish between different nuclear configurations corresponding to the associated fragment either in the ground or first excited states. The distance of about 30 meters between the breakup target and the detectors is large enough for those fragment to De-excite and they are always identified in the ground state. The distinction between ground and excited states could be done by looking for possible gamma rays coming from the fragments [6, 14, 15] (which decay very quickly, so we assume they did it inside the breakup target) produced at the middle focal plane during the experiment. The detection of these γ rays is the only part of the experiment that interests us in this work, but the analysis of the experimental results requires the complete identification and tracking of projectiles and fragments, and consequently needs other information additional to the specific γ ray detection.

1.2 Detector equipment for tracking and particle identification

In the following section a brief description of the detectors used in the measurement of the observables needed for the experimental analysis is done.

The last point will be dedicated to the γ rays detector, where a more detailed treatment is presented.

1.2.1 The tracking detectors: The TPC's

For the determination of the position in x and y of the projectiles and the fragments, Time Projection Chambers (TPC's) [18] were used.

The TPC's are P10 gas filled detectors operating at normal pressure and room temperature. They have four anodes and one cathode. The anodes are wires and there is a "delay line" just below them (see figure 1.3).
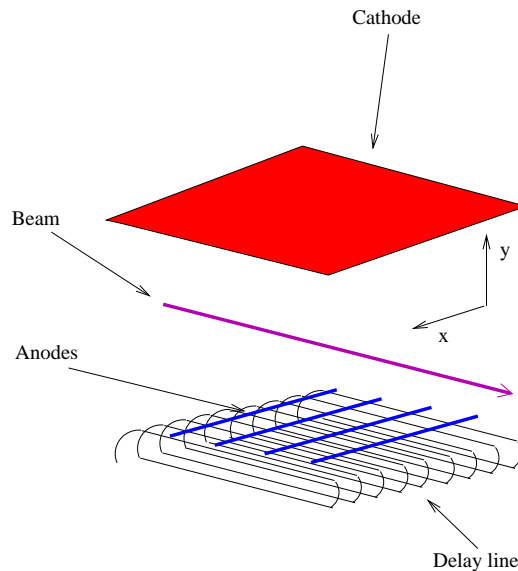

Figure 1.3: *Schematic view of a time projection chamber.*

An ionizing particle passing through the detector creates a shower of electrons along its track. These electrons drift towards the anode wires (the drift

time gives us the y coordinate information) and once near the wires they are accelerated under the effect of a radial electric field. The acceleration allows a maximum atomic ionization, producing a big shower of localized negative charge near the anode, which is reflected as positive in the delay line. The positive charge in the delay line produces a pulse which is collected and the time it takes to be collected can be used to deduce the position in x (see figure 1.4). From the x and y position measurement in two different detectors we could deduced the angle as well.
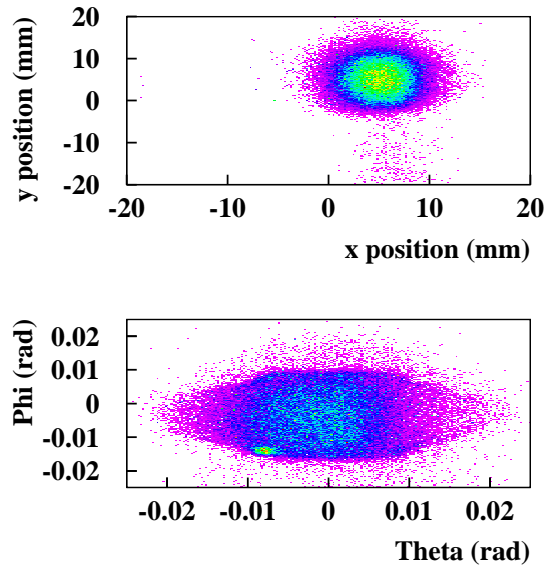

Figure 1.4: *Shape and angular dispersion of the beam at the breakup target position obtained by extrapolation of the information at the third and fourth TPCs. Theta is the angle in the x direction and phi is the angle in the y direction.*

These detectors have a position resolution in x and y better than 0.5 mm and they have a very small amount of matter in that minimizes the angular straggling.

An example of the tracking information that could be obtained with those detectors is presented in figure 1.4 for the particular case of ^{22}O. This position detectors allow us to obtain a very accurate measurement of the magnetic

rigidity (Bρ)in an event by event basis.

1.2.2   The ionization chambers

For the charge identification of the projectiles and the fragments, MUltiple
Sampling Ionization Chambers (MUSIC's) [19] were used.

A MUSIC is an ionization chamber filled with P10 gas (90% Ar, 10%
CH_4) at normal pressure and room temperature. The detector has an active
cross section area of 772.8 cm^2 and 4 anodes of 10.0 cm length each one (see
figure 1.5).

An ionizing particle that penetrates inside this detector generates a cloud
of gas ions and free electrons. The ionization is proportional to the square
of the charge of the incoming particle, and also depends on its velocity. The
produced electrons drift towards the anodes and the ions towards the cath-
ode. By getting the electron signal, which is proportional to the produced
shower, we can obtain the charge of the particle passing through if we know
its velocity.

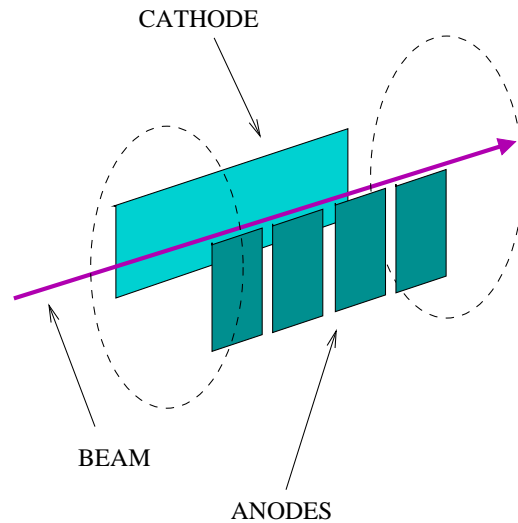The four anodes are used to have four different measurements to average
out.

Figure 1.5: *Schematic view of a MUSIC.*

1.2.3 The plastic scintillators

The plastic scintillators were used in the experiment as timing detectors, because of the fast rise time of the light pulse produced when charged particles pass through the plastic material.

The used scintillators were made of BC420 plastic 5 mm thick, and had two photo-multipliers (on the left and on the right side) to improve time resolution and to give position information as well.

The timing information provided by the plastic scintillators was used to obtain the time it took the produced nuclei to pass through the FRS, or Time Of Flight (TOF). This was done for the projectile (nuclei before the breakup target) by measuring the TOF of the projectiles between the first scintillator (located at the first focal plane of the FRS) and the second scintillator (located at the medium/second focal plane of the FRS), and for the fragments (nuclei after the breakup target) measuring the TOF between the second scintillator and the third one (located at the final/fourth focal plane of the FRS).

The TOF is a useful magnitude to obtain the velocity of the observed nucleus. The velocity is equal to the length of the path followed by the nucleus between two plastic scintillators divided by the TOF measured with the same scintillators. Once the value for the velocity of the nucleus and the magnetic rigidity ($B\rho$) are known, the ratio mass number over charge number (A/Z)can be deduced using the expression 1.1, β is the velocity of the nucleus in c units and γ is the Lorentz factor. If in addition we know the Z from the MUSICs measurement, the unambiguous projectile/fragment identification is possible (see figure 1.6 corresponding to the fragment identification for a setting centered on ^{20}O). The x axis corresponds to the mass-to-charge ratio and the y axis is the charge of the nucleus obtained with the music.

$$B\rho = \beta\gamma \cdot \frac{A \cdot u}{e \cdot Z} \tag{1.1}$$

1.3 The NaI Array for γ-detection

For the detection of the gamma rays coming from the projectiles after one nucleon removal, an array like the one presented in the figure 1.7 was used. It consists in 32 hexagonal NaI crystal detectors, which are scintillation detectors, disposed parallel forming a 'ring' around the beam axis.
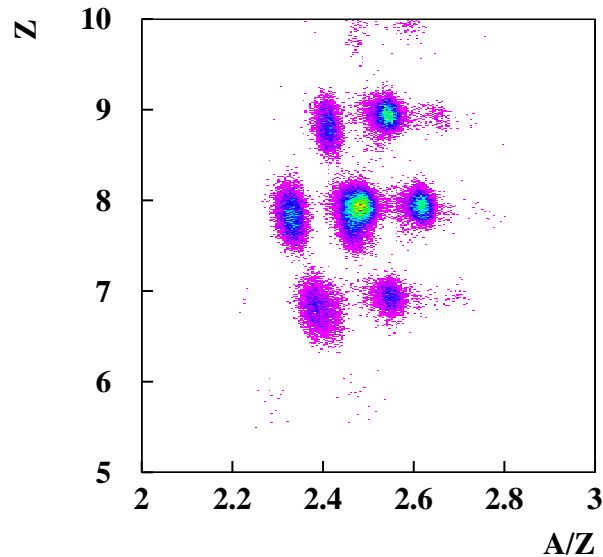
Figure 1.6: *Typical identification spectrum obtained from the charge (Z) measured in the MUSIC detectors and the A/Z ratio deduced from the TOF.*

A scintillation detector [20] has two important components: the scintillator and the photo-multiplier. The scintillator (a NaI crystal in our case) works by excitation of its atoms and molecules when some radiation passes through it undertaking different processes (photo-electric effect, Compton effect, pair production, ...), and consequent De-excitation by visible (or near-visible) light emission (this process can take a certain time which defines the response velocity of the scintillator). Further amplification of the light produced is done at the photo-multiplier by generating electrons at the cathode by photo-electric effect. These primary electrons are multiplied inside the tube (a typical gain is 10^6) and finally a big amount of electrons hits the anode and gives rise to an electric pulse proportional to the amount of energy deposited at the crystal. This means that scintillation detectors should have a linear stable response with energy, but some factors (mainly the photo-multiplication process and possible radiation damage in the crystal) can affect to these two important characteristics of the detector.
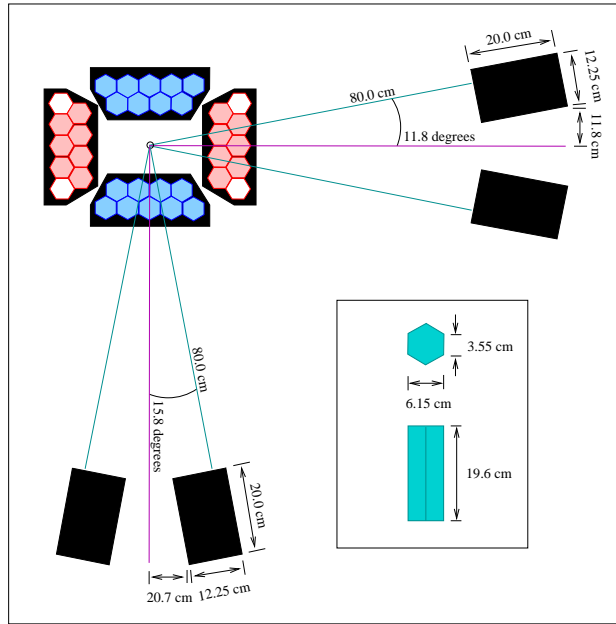
17

Figure 1.7: *The NaI array was made up of 32 individual NaI crystals (shaded hexagons in the figure), the dimensions of each one are given in the box (bottom, right). Three main views are represented: up, on the left, the front view; on the right, the side view; and down is the top view.*

The setup was designed to get the largest possible amount of the gamma rays emitted from the fragments. The angular distribution of the emitted γ rays with respect to the beam axis was peaked forward, due to the high energy, in the polar angle at around 16 degrees (approximately 0.3 radians) as can be seen in the figure 1.8. The individual NaI crystals were placed at this angle forming a 'ring' around the beam. At the same time, we try to get an equilibrium between avoiding the beam (see figure 1.9) and having the biggest possible geometric efficiency.

Very often a big amount of low energy γ rays coming from the background [16, 17] disturb our measurement. This number is proportional to the charge of the target and projectile and could be of relative importance up to energies around 500 keV. In order to reduce those background γ rays we placed a shielding in front of the NaI crystals consisting in one layer of aluminum (2.0 mm thick) and two layers of lead (each one 1.0 mm thick). These two materials have high interaction cross sections for low energy gamma rays
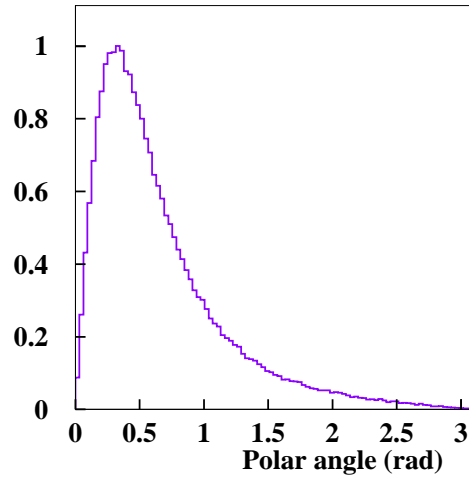
Figure 1.8: *Angular distribution with respect to the beam direction of the gamma rays emitted by a moving source at 1 GeV/nucleon ($\beta=0.8667c$). The maximum is found around 0.3 radians.*

(figure 1.10) and thus the mean free path for those γ rays in those materials is low. In consequence, 4.0 mm. are enough to reduce their intensity to an acceptable level for our purpose. As the emitted γ rays during the experiment are strongly Doppler shifted due to the high velocity of the emitter fragments ($\beta \simeq 0.876$), their energies, as seen by the detectors, are expected to be much higher than 1 MeV. This is not the case for the background γ rays, which do not suffer any Doppler shift and remain with low energy. With the Aluminum and Lead layers, the ratio between the number of γ rays before and after attenuation for γ rays of 10 keV is around 10^{-96} and for γ rays of 100 keV is of the order of 10^{-9}, but for γ rays of 1 MeV it is 0.8. In this way we obtain the desired reduction in the number of low energy γ rays, keeping the intensity of the high energy ones.

The main information obtained with this array is the energy released in each individual NaI crystal per event, and the time at which the event took place, having as origin for the time information the plastic scintillator before the breakup target.
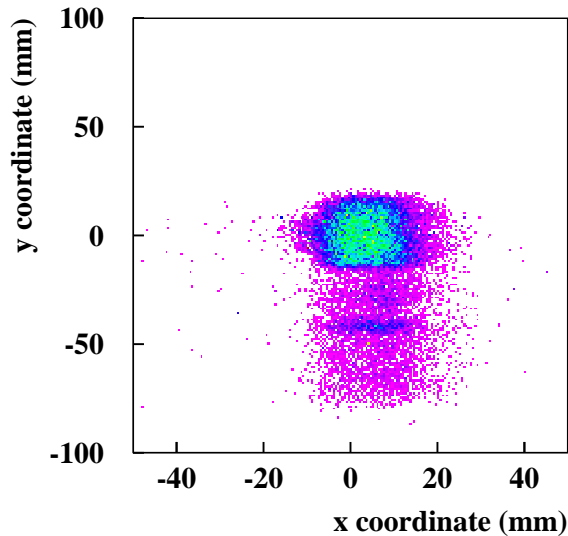
Figure 1.9: *The beam as it is seen by the NaI crystals array. The picture is obtained by extrapolation to the array position the beam image at the third and fourth TPCs (located before and after the NaI scintillators). The size of the beam justifies the dimension of the "hole" in our array.*

Energy information

The energy information in each crystal is needed to obtain the emitted gamma energy and the number of detected γ rays. The energy information from the emitted gamma rays is obviously Doppler shifted and must be corrected. It is possible to get the center-of-mass energy of the emitted gamma by looking at the energy of the event in each individual crystal and Doppler correcting it by taking into account the angle of the NaI crystal with respect to the emitter direction. This angle is obtained by simply measuring the position of the detector with respect to the breakup target (which is supposed to be the emission position) and the direction of the emitter nucleus given by the tracking detectors. There is an uncertainty in the measurement of the angle (approximately 4.5 degrees in the setup for our experiment)
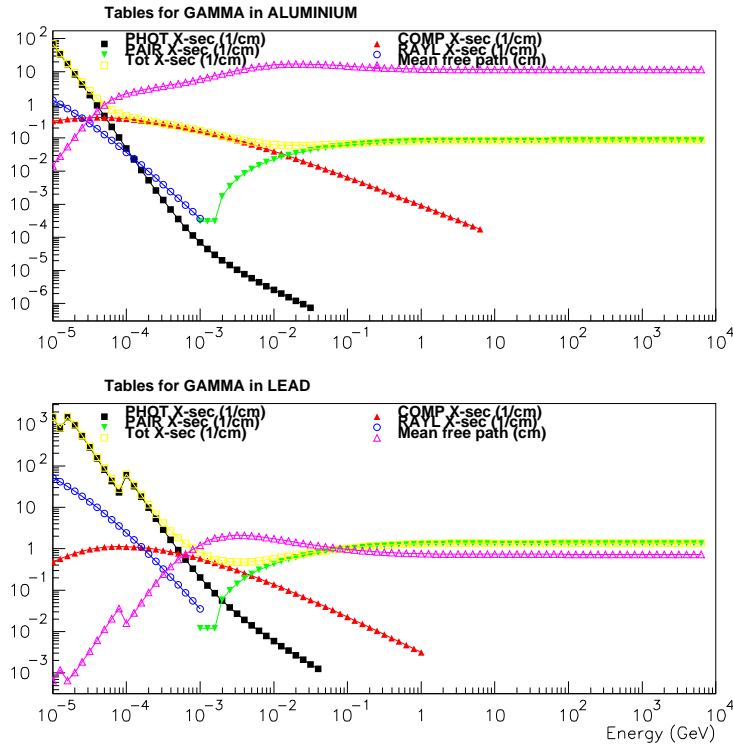
Figure 1.10: *Cross sections for different processes of the gamma rays in Aluminum and Lead (Phot. stands for photo-electric effect, Pair for pair production, Comp. for Compton effect, Rayl. for Rayleigh scattering, and Tot. refers to the total cross section). The mean free paths are also shown in the picture [21].*

which depends on the size and the position of the detectors. As they are not punctual, their position are conventionally taken in the center of their volume, here is the origin of the Doppler broadening and, as mentioned before in this work, it cannot be corrected. The nuclei excited at the breakup target which De-excite via γ rays are supposed to do it inside the target itself because the gamma emission is a very fast process [22] (of the order of 0.1 ns.) and at velocities of β=0.876, the fragments have reached only around 3 cm. from the emission point, which is negligible with respect to the 80 cm. that is the distance between the target and the array. Once obtained, the Doppler corrected spectra of all the individual crystals can be added without any problem to get the total array energy spectrum.
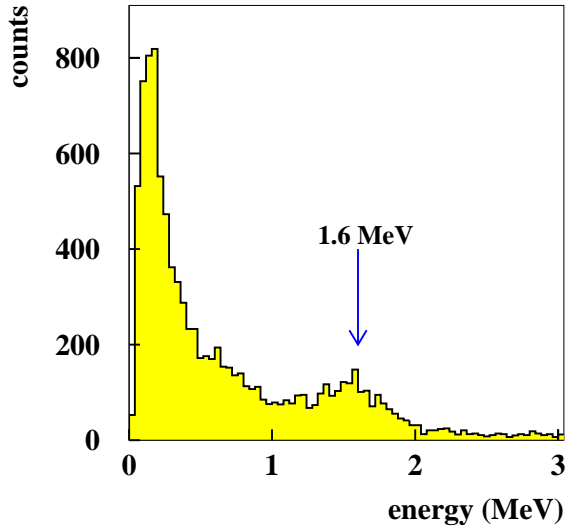
Figure 1.11: *Energy spectrum obtained for the γ ray emitted by the ^{20}O, produced at the breakup target after one neutron removal from ^{21}O. The peak is centered at 1.589 ± 0.012 MeV and has a widthness (FWHM) of 0.465 ± 0.032 MeV.*

In figure 1.11 we show the energy spectrum of ^{20}O obtained with the NaI array at the experiment, after Doppler correction. The peak is centered at 1.589 ± 0.012 MeV and has a widthness (FWHM) of 0.465 ± 0.032 MeV, what makes an energy resolution of around 29 %. Obviously, this low energy resolution is caused by the Doppler broadening effect. The measurement of the emitted γ ray in coincidence with the momentum distribution of the ^{20}O after one neutron removal from ^{21}O is very useful to study the nuclear structure by distinguishing the fundamental from the first excited state.

In the energy spectrum there are also contributions from the background γ rays and from other particles. It is important to remember that the energy for the background γ rays is low (because they are emitted at rest) and that they are practically absorbed by the layers of Aluminum and Lead in front of the NaI detectors, so we can conclude that the contribution from those γ

rays is negligible in the region of the spectrum were the information about the emitted γ rays is crucial. This does not happen with other particles and their contributions must be eliminated in other way.
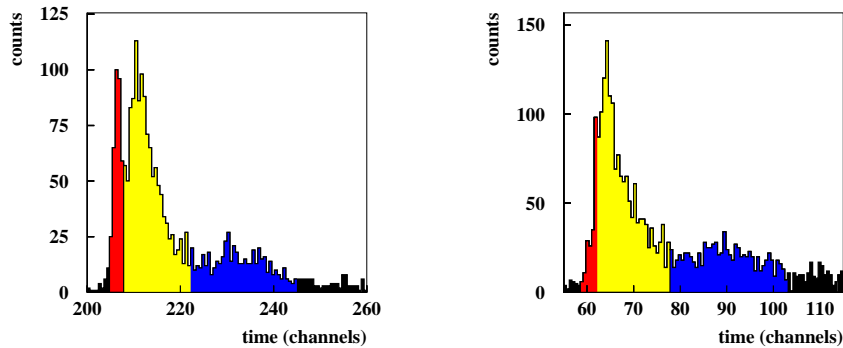
Time information

Figure 1.12: *Left: Typical time spectrum of one individual NaI crystal during the experiment. Charged particles, γ rays and neutrons contributions are showed in different grey: intermediate for the charged particles, lighter for the γ rays, and darker for the neutrons. In the analysis a window getting only the γ rays is set to reduce the background. Right: NaI crystal time spectrum with bad time resolution.*

The time information of the NaI detectors is used to discriminate γ rays (mainly coming from excited nuclei produced at the breakup target) from charged particles (mainly nuclei produced at or coming from the breakup target) and neutrons (which are ripped out of the nuclei in the breakup reactions). To be able to discriminate, the detector must have enough time resolution to distinguish the three contributions' peaks, specially the closest ones due to charged particles and γ rays. Typical time spectra obtained in our experiment are presented in the figure 1.12. The time spectra can be understood in the following way: coming from the interaction point, we have three kinds of particles, γ's, neutrons and charged particles. The fastest ones are the γ rays, and after then we have the the neutrons and the charged particles. The biggest shower is the one produced by the charged particles, followed by the one generated by the γ rays. The neutrons' shower is the

23

weakest. With these considerations the charged particles' shower is the first one seen, because though it comes later than the γ rays' one, it is bigger and is sooner detected. The next one is the γ rays', and finally, a not very high peak corresponding to the neutrons appears. By cutting in the γ rays' peak window we get only their contribution and the energy spectrum is clean of unwanted background. NaI detectors are fast enough to distinguish the neutrons from the charged particles and the γ rays in our experiment, but these two last peaks are sometimes difficult to be discriminated (see figure 1.12 right).
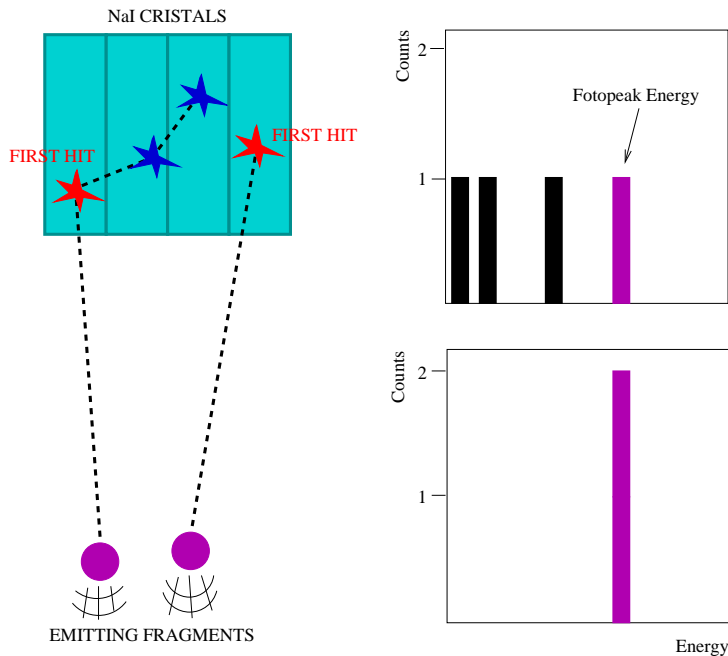
Figure 1.13: *Two nuclei emit two γ rays. The first one releases his energy on three neighbor NaI crystals, the second one is totally absorbed in the first hit. Without treatment (upper spectrum) only the second gamma contributes to the photo-peak. By adding the energy of the three detectors hit by the first gamma and assigning it to the first hit crystal we can recover the event for the photo-peak (lower spectrum). This procedure is known as Add-back.*

The time information can be extremely important for the analysis including add-back correction. With this correction we try to reconstruct gamma events which did not leave all their energy in the first hit detector, but only a part of it, and the rest energy is deposited in neighbor NaI crystals. The time

information gives us the moment of the collection of a certain energy in one scintillator. If we look at nearby detectors (usually four) as a whole by considering the energy of the real detected gamma the addition of the energies of these detectors, and assigning it to the first hit NaI crystal of the group of neighbors (this must be done before the Doppler correction) it is possible to gain in photo-peak efficiency without loosing in energy resolution: we are virtually using bigger detectors but the Doppler broadening is the same as for one individual crystal, because we assigned all the energy of the group of neighbor crystals to just one (the first hit of them), whose position is really the only one we must use for the Doppler correction as the γ ray was ejected in that direction). Figure 1.13 illustrates this procedure.
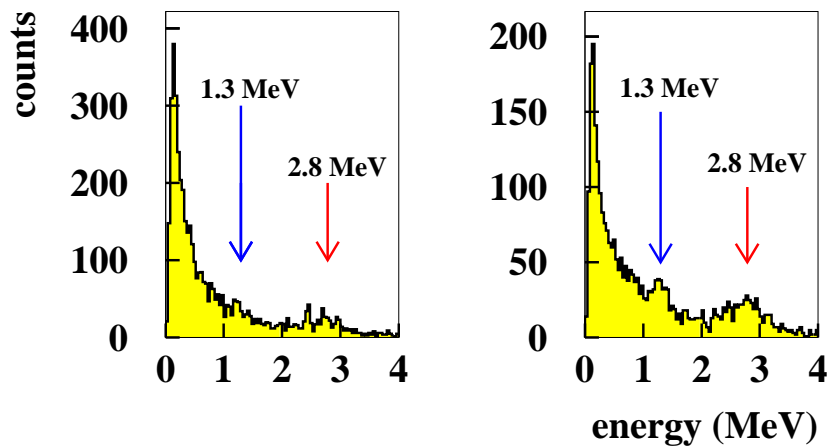
Figure 1.14: *Energy spectrum of the radiation detected at the whole array with applied windows in Z and A/Z to select the projectile ^{23}O that goes to the fragment ^{22}O, before (left) and after (right) the Add-back treatment. The Doppler correction has been done to obtain the γ rays energies in the emitter (^{22}O) reference system.*

In figure 1.14 we show the energy spectrum of the γ rays emitted by the ^{22}O ions De-exciting at the breakup target position. On the left, the

spectrum obtained after the Doppler correction is presented. To show the usefulness of the Add-back procedure with a real case, on the right we show the same spectrum after Add-back and Doppler correction. The peaks at 1.295 ± 0.022 and 2.783 ± 0.024 MeV (corresponding to the γ De-excitation of the second excited state to the first one, and to the De-excitation of the first excited state to the fundamental one, respectively) are much more clear after applying the Add-back treatment.

We want to stress the importance of this last result. The γ energy spectrum of ^{22}O was not known experimentally. The two γ rays observed in this experiment are novel information about the excitation scheme of ^{22}O.

We propose for ^{22}O the level scheme shown in figure 1.15.
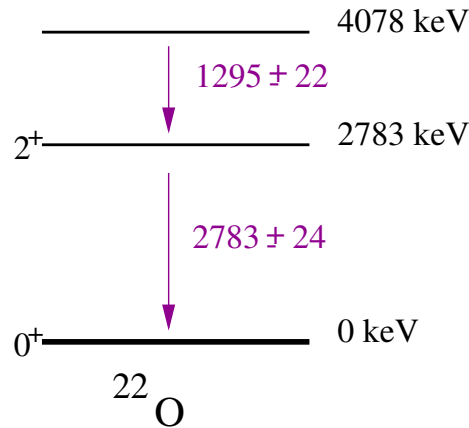
Figure 1.15: *Level scheme proposed for ^{22}O.*

^{22}O was also studied in an almost contemporaneous experiment performed at GANIL at intermediate energies (≈ 75 MeV/nucleon) [9]. The results of both experiments are in good agreement: the γ rays energies obtained at GANIL are around 1.3 and 3.1 MeV, while ours are around 1.3 and 2.8 MeV. Note that there is a small discrepancy for the assignment of the higher energy γ ray. This can be explained by the fact that in our case the photo-peak will be strongly merged at those energies with the upper edge of the Compton background that lies very near after Doppler correction. In addition, the photo-peak will be really small at those energies. These two factors make very difficult to distinguish both contributions, and the resulting "peak" appears at a slightly lower energy. This effect was checked with a simulation,

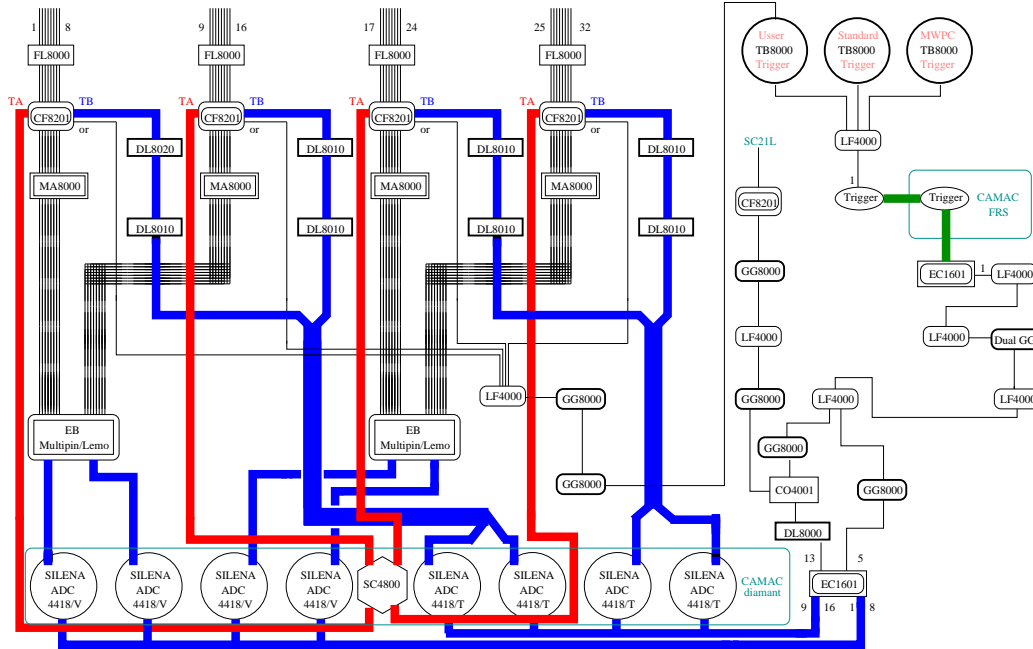Figure 1.16: *Electronics for the NaI array. The used modules include fast linear amplifiers (FL), constant fraction discriminators (CF), main amplifiers (MA), analogic to digital converters (ADC), delays (DL), time to digital converters (TDC), coincidence modules (CO), fan in/fan outs (LF), gate generators (GG), and a scaler (SC).*

where a 3.0 MeV γ ray was emitted and a peak (mixture of Compton edge and photo-peak) at 2.8 MeV was observed in the spectrum after Doppler correction.

The associated electronics

The electronics controlling the array is shown in the figure 1.16. The signals coming from the individual NaI crystals are first amplified inside the cave where the experiment was taking place using fast linear amplifiers, once outside, they pass trough constant fraction discriminators, and are further amplified with main amplifiers, and converted to digital by means of ADC's. At the same time the signal coming from the constant fraction discriminators is used as trigger, and as stop for the time signals in the TDC's (whose start is given by the coincidence between a registered signal in the plastic scintillator just before the breakup target and a valid trigger).

Chapter 2

Data analysis

The analysis of any nuclear physics experiment nowadays is not a trivial task. The difficulty comes mainly from the number of electronic channels involved. The complete analysis of the experiment that was briefly introduced in the chapter 1 contains more than 150 electronic channels. From them, very valuable information as the complete identification, position and angular information for projectiles and fragments on an event by event basis was obtained.

As it was already explained, in this work we are mainly interested in the characterization of the detection of γ rays emitted by a relativistic source. Consequently, we will concentrate on the evaluation of the signals recorderd by the γ detectors used in this experiment. As introduced in the previous chapter, this detector consists of an array of 32 NaI crystals. In order to extract physical information from those detectors several calibrations were necessary. These calibrations were done with different standard γ sources along the experiment that was running during 3 weeks in order to ensure the stability of our calibrations. A detailed description of the calibration related to the NaI crystals array and its associated electronics is presented in this chapter.

2.1   Calibration of the electronics

2.1.1   TDCs' calibration

The time information collected with the NaI detectors is used in the experiment to set time windows to discriminate γ rays from charged particles and

neutrons (figure 1.12).

This time information was converted to digital with Time to Digital Converters (TDC). See figure 1.16.

We performed a time calibration to obtain the time information in time units instead of channels.
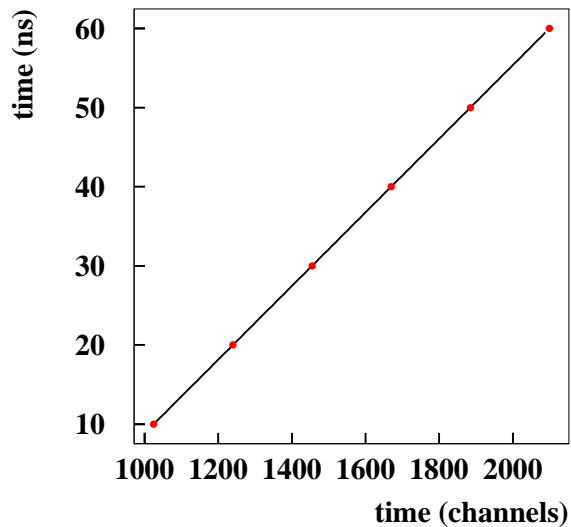

Figure 2.1: *Time calibration of the TDC used in the experiment. The error bars are smaller than the size of the points.*

A time calibrator was set to give a pack of pulses with a period of 10 ns over a range of 320 ns. The time calibrator was connected to every TDCs channel. A linear fit relating channels and time information provides the calibration as presented in the figure 2.1

2.2 Calibrations with radioactive sources

The calibrations that are presented in this section were done at the beginning and at the end of the experiment to check the stability of the detectors and to ensure the validity of the calibrations over the time. The elapsed time for each measurement was around one hour and a half.

Those measurements focused on different aspects of the energy spectra for each one of the NaI detectors: energy calibration, energy resolution dependence with the energy, and absolute efficiency calibration.

For this purpose different γ sources were used. They were placed at the breakup target position (80 cm. from the detectors). The analysis was done using the energy spectrum of each individual detector. In order to have a good range of validity for the calibrations, the sources had to emit high energy γ rays (in the experiment, the energies of the γ rays emitted from excited nuclei are going to be very high as a consequence of the Doppler shift effect). We need high energy γ rays, otherwise the error in the extrapolation of the energy calibration can be unacceptable). In addition, the source needs to be intense enough to allow a reliable efficiency calibration (the efficiency of the NaI detectors at those energies is very low and if the intensity of the radiation is not very high we will not be able to distinguish the photo-peak from the background).

The energy calibration and the energy resolution dependence with the energy are important for the complete analysis of the experiment, but the key piece is without any doubt the efficiency calibration, basic to obtain the real number of excited nuclei produced at the breakup target. This information is crucial to discriminate the last neutron wave function of the nuclei under study in a particular state (remember that is the ultimate goal of the whole experiment).

Two sources were chosen for the calibrations:

- A ^{88}Y source, which decays via $\beta+$ to ^{88}Sr, emitter of two γ rays of 898 and 1836 keV. The branching ratios for these γ rays are 0.94 and 0.99 respectively. The intensity of this source at the beginning of the experiment was 333 kBq.

  The decay scheme for this source is represented in the figure 2.2 [1].

- A ^{56}Co source, decaying via $\beta+$ to ^{56}Fe, which can emit different γ rays being the most important contributions: 847 keV, 1238 keV, 2598

keV, 1771 keV, 1038 keV, 2035 keV, 3253 keV, 1360 keV, 2015 keV, 3202 keV, 1175 keV and 3273 keV (ordered by their intensity). The branching ratios for those γ are: 1.0, 0.68, 0.17, 0.16, 0.14, 0.079, 0.079, 0.043, 0.043, 0.031, 0.032, 0.023 and 0.019 respectively.
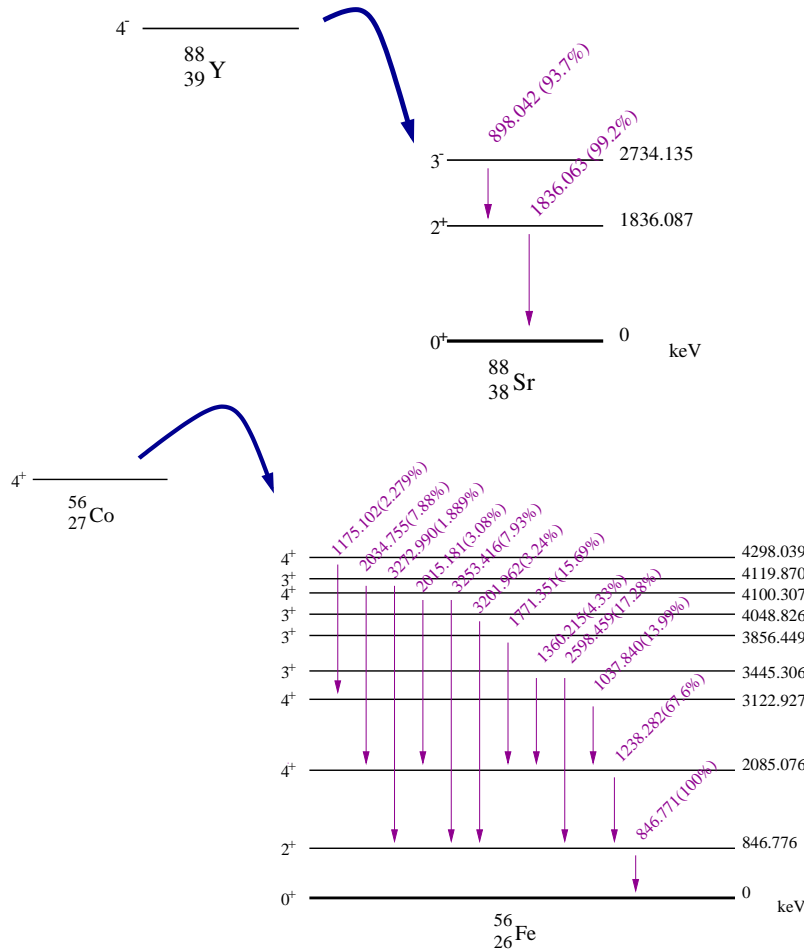
Figure 2.2: *Top: Decay scheme for the ^{88}Y source. Bottom: Decay scheme for the ^{56}Co source taking into account only the main γ's emitted.*

Only the most intense γ rays in the list above were used, in order to work with clear peaks for a better calibration. This includes the 847 keV, the 1238 keV and the 2598 keV γ rays and the combination of the 3253, 3202 and 3273 keV γ's (with an effective branching ratio of 0.13), which are undoubtedly superposed in the energy spectra due to the limited resolution of the detectors. This source had a strength of 454 kBq at the beginning of the experiment. The decay scheme for this

source, considering only the main contributions to the gamma spectrum of the ^{56}Fe, is represented in the figure 2.2 [1].

2.2.1 Energy

We used Analog to Digital Converters (ADC) to process the energy information (figure 1.16), converting it to digital before entering the acquisition. We present a characteristic energy spectrum with a typical "calibration" fit in the figure 2.3. In this particular case, the source is ^{88}Y. The two peaks in the spectrum correspond to the γ rays at 898 and 1836 keV, and are fit to Gaussians. At the same time, the background is fit to a third degree polynomial, and the Compton edge to another Gaussian.

Figure 2.3: *Energy calibration spectrum. The gamma source used in this case, ^{88}Y, decays via $\beta+$ going to ^{88}Sr, emitter of 898 and 1836 keV γ rays. Those energies for the emitted γ rays correspond to the two main peaks in the histogram, which are fit to Gaussians. At the same time, the background is fit to a third degree polynomial, and the Compton edge to another Gaussian.*
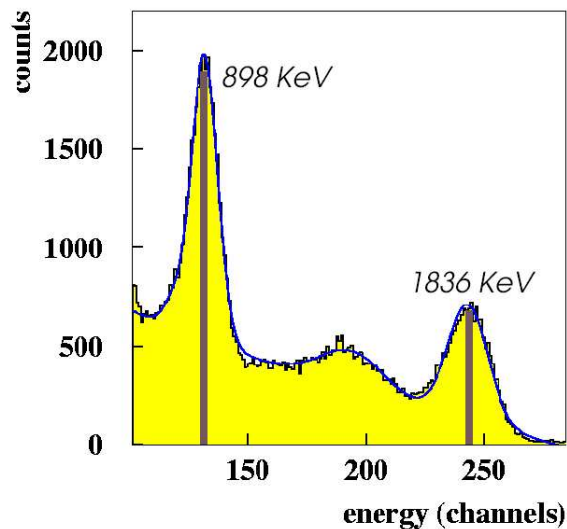
We observed during the experiment a shift in the relation between a certain channel in the spectrum and the corresponding energy (see figure 2.4). We suspect that the observed shift is mainly due to radiation damage in the NaI crystals: the prolonged exposure to intense radiation during the experiment caused a decrease of the optical transmission in the crystals and a reduction in the produced pulse height, shifting towards lower channels gradually with time.
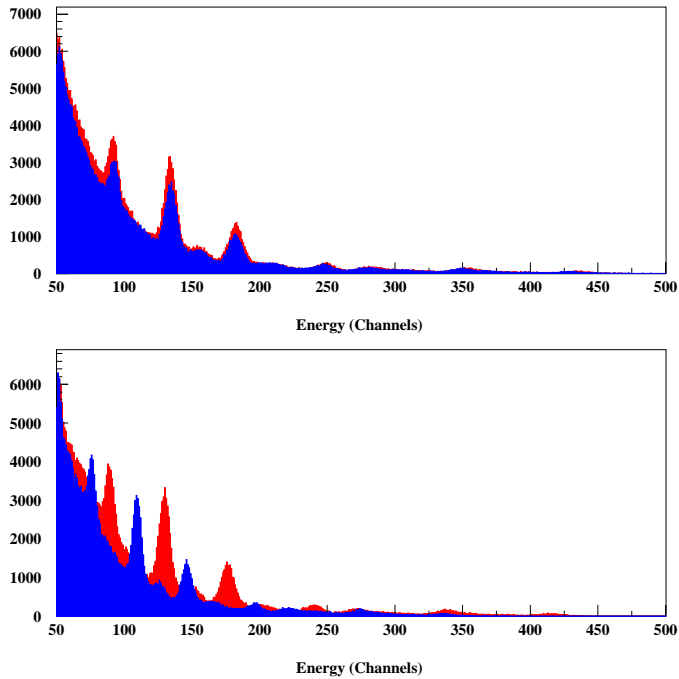
Figure 2.4: *Examples on how the energy-relation-with-channel changed with the time. Grey color refers to calibrations done at the beginning of the experiment. Black color is for the ones done at the end. In the histogram above we have a detector stable with time. The histogram below shows the most common case: a shift in the relation between the energy of the peaks and the associated channel. In this example the source used is* ^{56}Co.

The ideal solution to correct the problem would be to have a "pulser" providing a permanent signal to take as a reference all over the experiment. In this way, if the shift effect appears, it is possible to measure its magnitude

by using the displacement in the signal provided by the "pulser".

Unfortunately, we did not have a pulser for constant monitoring. In order to correct this problem we suppose that the variation happened gradually and had a linear dependence with time (we use this assumption because we only have two reference points). We obtained in this way a time dependent energy calibration.

The final result obtained for the energy calibration for an individual NaI crystal of the array is presented in the figure 2.5. The nice linear fit shows the linearity of the detector response with the energy.
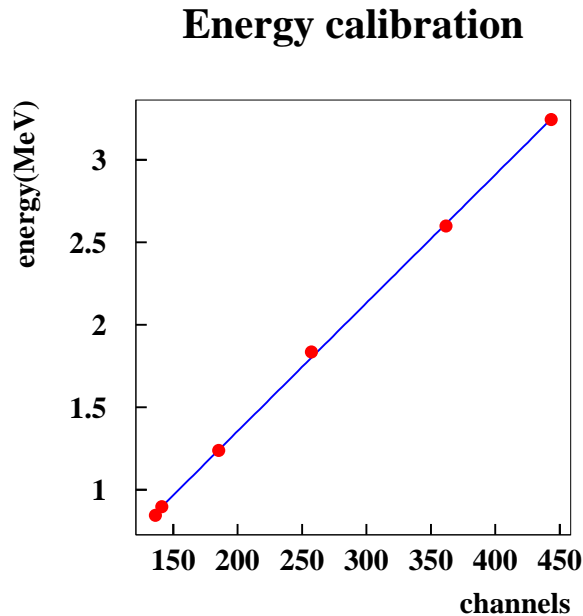
Energy calibration

Figure 2.5: *Plot of the linear fit done for the energy calibration of one typical NaI crystal of the array. The points used correspond to γ rays from ^{88}Y and ^{56}Co sources. The error bars fall inside the points.*

2.2.2 Energy resolution

The energy resolution is an important characteristic of a γ ray detector related to its ability to discriminate between γ with slightly different energy. The contributions to the energy resolution (ΔE) of a NaI crystal are mainly three [24, 25]. The first one is due to the scintillator itself (ΔE_{sci}), and depends on the way the γ rays react before depositing all their energy (only one photo-electric interaction, several Comptons, one Compton and one photo-electric interaction, ...). In other words: The intensity of the light emitted by the crystal depends on the energy. The second term$(2.35 \cdot \sqrt{N_{phot}})$ is statistical and is related to the photo-multiplication process (in first approximation this smearing is proportional to the square root of the number of photoelectrons produced at the photo-cathode). The last term ($K \cdot E_\gamma$, being K a constant dependent of the detector, that in our case is approximately equal to 0.1) includes inhomogeneities in the scintillator and the photo-cathode and the spread in the light collection efficiency in the scintillator. This term depends linearly with the energy. The formula 2.1 shows these three contributions.

$$(\Delta E)^2 \simeq (\Delta E)^2{}_{sci} + (2.35 \cdot \sqrt{N_{phot}})^2 + (K \cdot E_\gamma)^2 \qquad (2.1)$$

To study the energy resolution dependence with the energy we used energy spectra like the one presented in the figure 2.3. The observables were the Full Width at Half Maximum of the Gaussians to which the photo-peaks were fit. The dependence extracted from this information is shown in the figure 2.6 for a typical crystal. The experimental data show a linear dependence that we understand since the most important contribution to the resolution at high energies is the third term of the formula 2.1. The errors assigned in figure 2.6 are larger for higher energies. At these energies the NaI efficiency is quite low and it is very difficult to distinguish between the photo-peak and the background (see figure 2.7 for the ^{56}Co source).

The typical energy resolution at 1330 keV for a standard NaI detector is known to be around 6 % ($\frac{\Delta E}{E}$), value similar to the one obtained in our measurements (around 10 % for most of the NaI detectors in the array, including the electronic channel smearing). This information about the dependence of the energy resolution with the energy for each individual crystal was lately used in the simulation to generate a more realistic response of the NaI crystals.

These are the main dependences for stopped sources. With moving

FWHM dependence
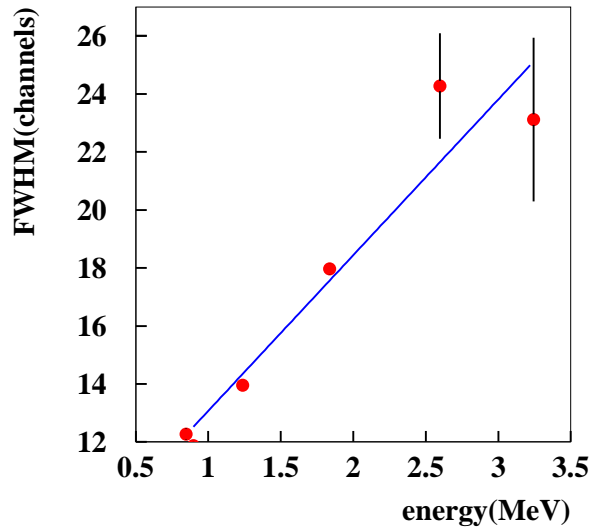
Figure 2.6: *Plot of the linear fit done for the energy resolution dependence for a typical NaI crystal of the array. The points used correspond to γ rays from ^{88}Y and ^{56}Co sources. The fit becomes worse as we go to higher energies, this is because at those energies the NaI detectors efficiency is quite low making very difficult to distinguish between the source and the background, as can be easily seen in the figure 2.7, where the fit for the higher γ rays taken into account of the ^{56}Co source is shown.*

sources the Doppler broadening represents another contribution to the energy resolution that must be taken into account in our analysis:

The γ rays emitted by the moving fragments after the breakup reactions are going to be Doppler shifted and the uncertainty in the angular direction of a γ ray will produce a wider photo-peak in the NaI detector (Doppler broadening) after the Doppler correction. This effect superposes to the normal energy resolution of the detector and, depending on the Doppler shift magnitude, can be the most important contribution. If this is the case, the observed energy resolution of the detector will be mainly the one due to the Doppler broadening.
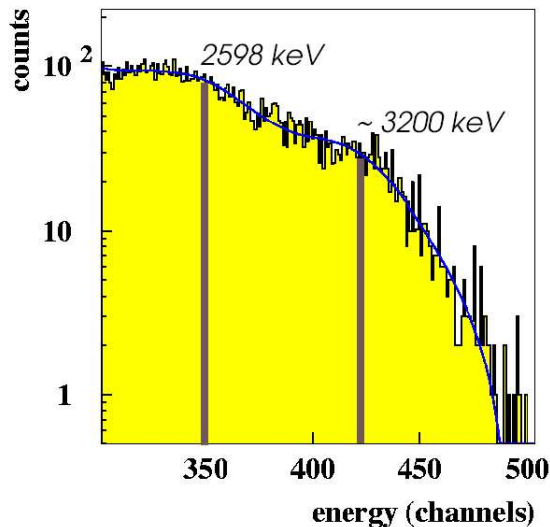
Figure 2.7: *Energy calibration spectrum for the higher energy γ rays of the ^{56}Co source. The two peaks are for the 2598 keV and the superposed 3253, 3202 and 3273 keV γ rays. At those energies, the NaI detectors efficiency is quite low and makes very difficult to distinguish between the source and the background.*

2.2.3 Detection efficiency

An important characteristic of the detectors we used is their efficiency. There are several definitions for the detection efficiency, some of them interrelated. The most commonly used is the total efficiency, and it is defined as the ratio between the number of detected events and the number of total events. It is a magnitude dependent not only on the energy, but also on the position, size and shape of the source and the detector. In the bibliography the information about this efficiency is related to measurements done for standard configurations. In our experiment it was necessary to evaluate the total efficiency for each NaI detector experimentally from a stopped source emitting γ rays at different energies and located at the breakup target position. This is the starting point to obtain the total number of γ rays emitted by the moving fragments at the breakup target.

The total efficiency depends also in the way the source emits. If the angular distribution of the radiation emitted by the source changes, the total efficiency will also change, because more (or less) radiation can be sent now to the detector. In this way, variations in the velocity of the γ rays emitter will modify the angular distribution of the emitted γ rays (figure 2.8) and the total detection efficiency. The way in which the angular distribution of the radiation affects the total efficiency depends on the position, size and shape of detector and source.
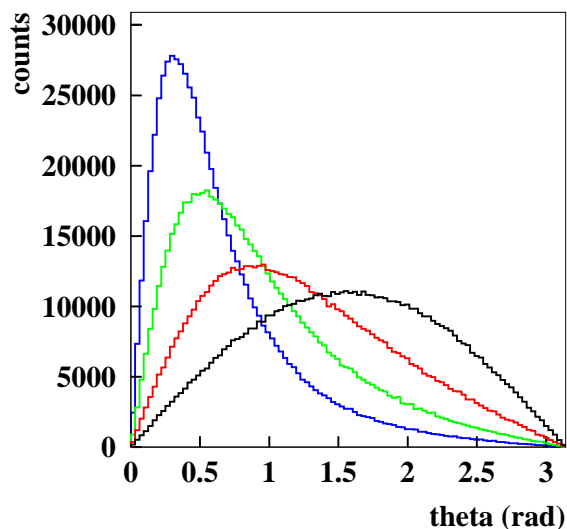
Figure 2.8: *Variation in the angular distribution with respect to the beam direction of the emitted gamma rays for different velocities of the emitters. From left to right: $\beta=0.87c$, $\beta=0.7c$, $\beta=0.4c$ and $\beta=0.0c$. All the curves have the same area.*

These dependences mentioned above, cause the division of the total efficiency concept into two: the geometric efficiency and the intrinsic efficiency. The geometric efficiency represents the part of the total efficiency which does not depend on the energy. It is defined as the ratio between the amount of radiation that reaches the detector volume (whether it is detected or not) and

the total amount of radiation emitted. The intrinsic efficiency only carries the energy dependence of the total efficiency and is defined in a standard way as the ratio between the total and the geometric efficiency. The intrinsic efficiency is also very used in the bibliography together with the total efficiency standard calibrations because it is independent on the particular conditions of the setup.

The efficiency calibration information done with stopped sources cannot be used in a direct way to obtain the total efficiency for moving sources because the angular distribution of γ rays emitted at rest is very different from the distribution of γ rays emitted from a moving source. This explains the necessity we have to simulate the total efficiency for the γ rays coming from moving emitters seen in the experiment. In another hand, the analysis of the experimental efficiency for radioactive sources is very important to show the validity of our simulation.
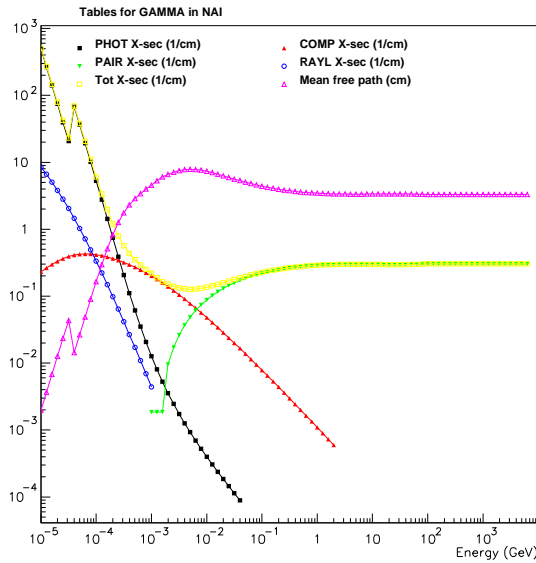

Figure 2.9: *Cross sections for photo-electric [21], Compton and pair production effects of gamma rays in NaI. The interaction length is also shown.*

To obtain the experimental efficiency response for the whole array we used the equation 2.2. In this equation, the total efficiency (ϵ_t) is calculated

using the area of the Gaussian fit to the photo-peak ($S_{\gamma i}$), the time duration of the calibration measurement (t), the scaling down factor between the total events in the detector and the events we order the acquisition to treat (f), the measured activity of the source in the day d_0 (A_0), the day of the calibration measurement (d), the half life of the source in days ($T_{1/2}$), the branching ratio of the gamma (BR_γ) and the dead time: the quotient between the events we order the acquisition to treat and the events the acquisition is really able to process (δ).

$$\epsilon_t = \frac{\frac{\sum_{i=1}^{32} S_{\gamma i}}{t} \cdot f}{A_0 \cdot e^{\frac{-ln2(d-d_0)}{T_{1/2}}} \cdot BR_\gamma \cdot (1 - \delta)} \tag{2.2}$$

The experimental values obtained for the total efficiency of the whole array at different energies are shown in the table 2.1. It can be seen that the total efficiency is lower at higher energies. This is caused by the variation of the intrinsic efficiency (the geometric efficiency is always the same, since we are using isotropic sources and we have not changed the setup).

Table 2.1: Experimental total efficiency dependence with energy obtained from the calibrations done with the ^{88}Y and ^{56}Co sources.

Energy (keV)	ϵ_t (%)
847	0.36
898	0.36
1238	0.23
1836	0.21
2598	0.14
3243	0.08

The variation of the intrinsic efficiency with the energy is related to the total interaction cross section of a γ ray in NaI (in this case), since this cross section is proportional to the probability of the gamma to interact with the crystal. If a γ ray interacts with the scintillator until all its energy is absorbed, it is detected. So, the higher the interaction probability is, the higher the detection efficiency results.
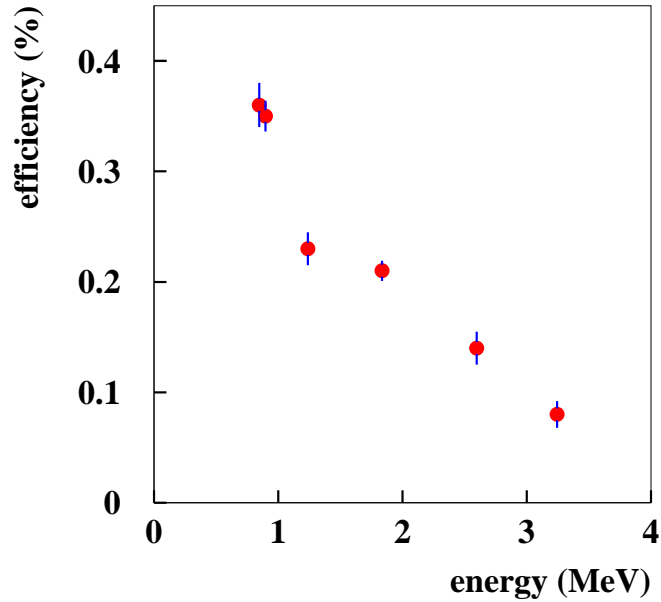
Figure 2.10: *Total efficiency dependence of the whole array with the energy.*

In figure 2.9 we present the cross sections for the most important processes where a γ ray can be involved inside the NaI crystal. The total cross section for energies between 800 and 4000 keV decreases with energy This explains the behavior observed for the intrinsic efficiency. A graphical representation of the total experimental efficiency as a function of the γ ray energy can be seen in the figure 2.10.

Chapter 3

The simulation tool

As we have seen in chapter 2, the total efficiency of our γ detector depends on the kinematical characteristics of the emitter which will determine the angular distribution and the Doppler shift of the observed γ rays. To take into account these effects we need a simulation of the process.

In this chapter we will present the simulation done with the code GEANT 3.21 for the NaI crystals array. GEANT [21] is a simulation tool based on a Montecarlo code developed at CERN that simulates the passage of elementary particles through the matter. It has a lot of applications in a wide variety of scientific areas. The version 3.21 is written in FORTRAN language (René Brun and Andy McPherson) and has received many contributions from scientists around the world, which, together with the feedback from the users to the authors and maintainers at CERN resulted in a great improvement of the system.

Our goal is to reproduce as accurately as possible the behavior of the real detector under certain conditions (i.e. total efficiency for radioactive sources at rest) in order to make predictions for other possibilities (i.e. total efficiency for moving sources). To accomplish this goal, the main characteristics describing our detectors obtained from the calibrations of the array, already shown in the previous chapter, are used as input and as cross-check to test the validity of our simulation.

In this way, the simulation process has two different stages: The first one linked to the experimental calibrations performed with the ^{88}Y and ^{56}Co sources, serves to adjust the simulation to the real experimental conditions. The objective in this part is to reproduce with our simulation the experimental results described in the last chapter. The second stage refers to

the predictions obtained from the simulation for the total, geometric and intrinsic efficiencies of the array for γ rays emitted at the target position by moving nuclei emerging from a breakup reaction. Those predictions are very important values needed for the complete analysis of our experiment and impossible to be obtained in another way. Although the second phase is the most interesting because it justifies the simulation, we want to stress on the necessity of a faithful reproduction of the physical interactions that take place in the detection process, together with specific aspects related to technical characteristics of our NaI detectors. This two stages are going to be developed separately in this chapter.

3.1   Motivation

The main reason to simulate the gamma detection with our array is to obtain a very precise dependence of the simulated array efficiency with the energy of the incoming gamma (efficiency response of our detector). We need it because during the experiment, due to the Doppler shift effect, really high energy γ rays are detected. The angular distribution of these γ rays depends mainly on the velocity of the emitter (so it is not isotropic like in the calibrations, and could be different for each considered case). As we have no way to determine an experimental efficiency calibration for those relativistic γ rays we need to get it from the simulation. To ensure the validity of the simulation the best is to compare the results with the experimental information when it exists. The first requirement is to include in the simulation all the experimental dependences and values obtained from the data analysis (i.e. realistic energy resolution, ...). With this starting point we have to check the agreement between experiment and simulation for low energy γ rays coming from a radioactive source at rest. The quality of this agreement would allow us to believe that our simulated efficiency at high energies for γ rays coming from relativistic moving fragments is realistic and can be used later on in the experiment.

3.2   Simulation design

We describe in this section all the elements introduced in the simulation. We will present first general considerations taken into account for a realistic description of the simulation to finally distinguish between the peculiarities

for at rest radioactive and moving sources.
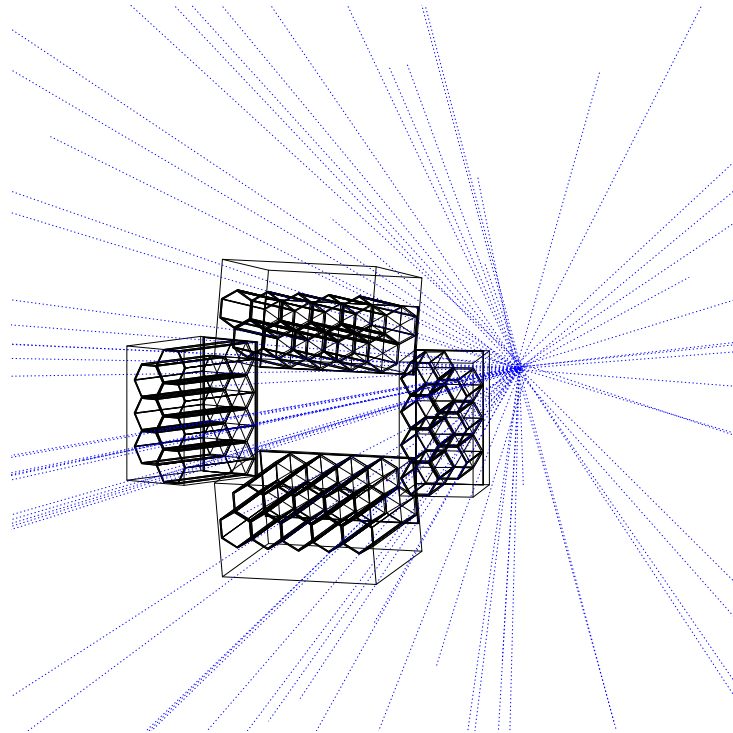
Figure 3.1: *The NaI crystals array simulated with GEANT 3.21. The geometry description of the simulation follows the technical characteristics presented in the figure 1.7*

For the NaI array definition, the geometry and materials were taken from the technical specifications for the detector (see section 2.2.4). The air atmosphere enveloping the setup and the Aluminum and Lead shieldings located in front of the NaI crystals, were also considered (see figure 3.1).

In the real setup there is a Time Projection Chamber placed between the target position (or γ emission point) and the array (see figure 1.2). The simulation does not include this detector. It does not represent any problem for the gamma transmission because such a detector is mainly P10 gas. Gamma rays pass through that detector easily since the typical interaction length in air for a 1 MeV gamma is around 100 meters as can be seen in the figure 3.2, and the detector thickness is around 10 cm. Due to the low density of gases under normal conditions the emitted γ rays rarely find a gas molecule to interact with.
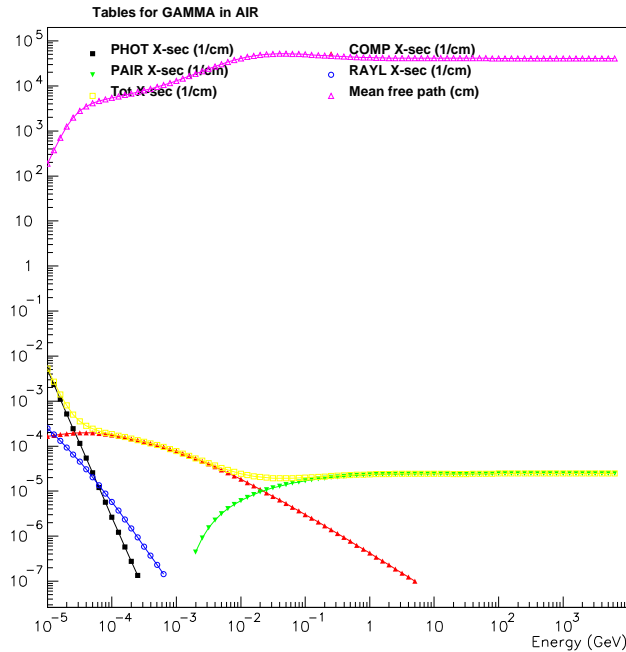
Figure 3.2: *Cross sections [21] for gamma rays in air under normal conditions. The interaction length is also shown.*

The treatment of the energy resolution dependence with the energy for the individual NaI crystals is also common to both stages. In the same way, the definition of the possible interactions between γ rays and matter is also common. The simulation includes the following processes: photoelectric effect, Compton scattering, pair production, bremsstrahlung, continuous energy loss (charged particles), multiple scattering, delta rays production, electron-positron anniquilation and Rayleigh scattering.

3.2.1 Radioactive sources at rest

In this stage we want to reproduce the results obtained in the experimental calibration phase (see section 2.2.3).

The specific definitions for the first stage of the simulation make reference to the emitter characteristics. We defined a punctual source at rest ([88]Y or [56]Co) located at the breakup target position emitting isotropically its principal γ rays. These γ rays are characterized by their energy and their emission probability (branching ratio) at each time. For a detailed description consult

section 2.2.

3.2.2 Moving sources

In this case moving sources are simulated. In order to have a realistic description of those moving sources we took into account some important things.
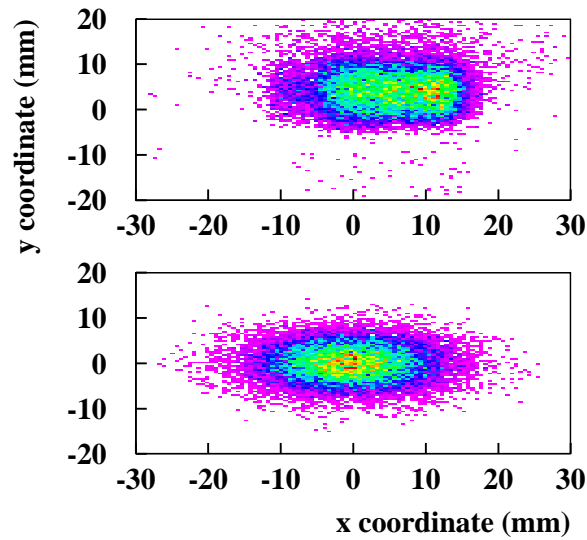
Figure 3.3: *Comparison between the beam spot at the target position as seen experimentally by the TPC's (top) and the beam size that we used for our simulation (bottom).*

The sources now are not emitting at rest with respect to the laboratory reference system. They have a relativistic velocity set in the simulation to 0.867c (typical value for the fragment nuclei velocities during the experiment). This velocity disturbs the isotropic distribution in the γ rays emission towards the forward direction, so, the corresponding peaked forward angular distribution (as the one presented in the figure 2.8) is considered.

In addition the γ rays are going to be Doppler shifted to higher energies. In other words, they will suffer from very low detection efficiency at
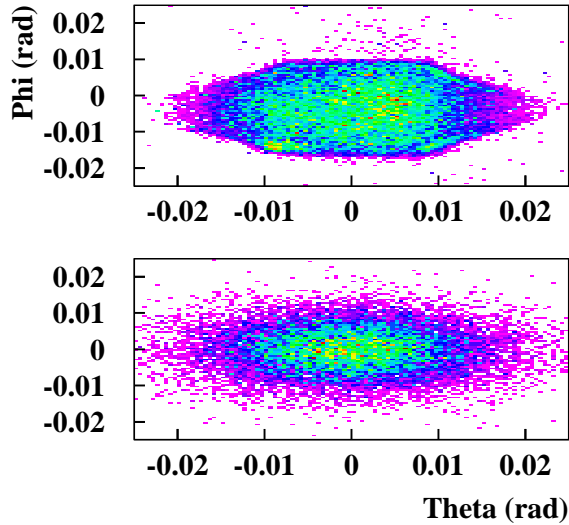
Figure 3.4: *Comparison between the angular divergence of the beam at the target position obtained from experimental measurements (top) and the one used for the simulation (bottom).*

the NaI detectors. Our simulation will ensure a Doppler correction similar to the experimental one. The goal is to simulate γ rays coming from the fragments produced after breakup. The γ emitter is not a source located in a fixed point any more. The beam spot at the breakup target has a spatial extension that is included in the simulation introducing a Gaussian smearing in x and y for the source position. In the same way a Gaussian smearing in the incident angle θ and ϕ for the source direction simulating the angular divergence of our experimental secondary beam is included. Finally we include a Gaussian smearing in the velocity of the source, centered in 0.867c. This β smearing takes into account the energy loss and straggling of the real fragments in the experiment. We have evaluated all those observables (beam spot, beam divergence and β distribution) from the experimental analysis of the data. The different parameters of the simulation were set in order to reproduce the experimental ones and ensure the quality of our predictions. The figures 3.3, 3.4, and 3.5 present a comparison between the measured and the simulated beam spot, beam divergence and β distribution respectively.
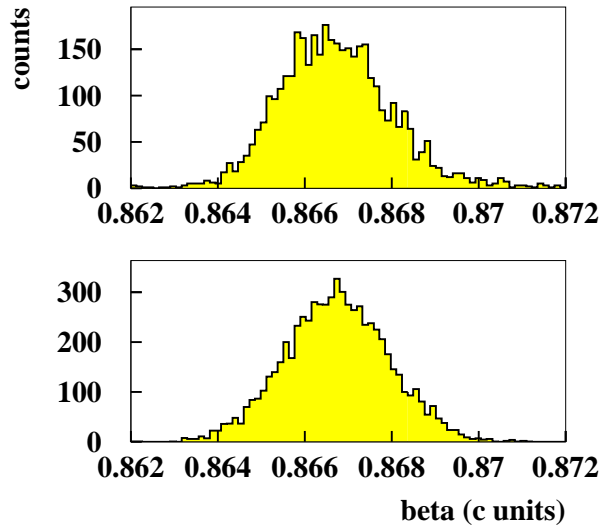
Figure 3.5: *Comparison between the fragment velocity distribution measured in the experiment (top) and the simulated one (bottom). This particular case corresponds to the fragment ^{22}O.*

3.3 Simulation results

The most important information that can be obtained from the simulation are the values for the total, geometric and intrinsic efficiencies in the two stages. It is important to know that experimentally we can only measure the total efficiency. In this case, the possibility to distinguish between the different contributions in the simulation can be very useful for the results interpretation. The total efficiency can be determined by the ratio between the total number of detected γ rays that fill the photo-peak corresponding to a certain γ energy in the spectrum ($N_{d\gamma}$), and the total number of emitted γ rays at that energy ($N_{e\gamma}$).

$$\epsilon_t = \frac{N_{d\gamma}}{N_{e\gamma}} \tag{3.1}$$

The geometric efficiency can be known by just dividing the total number

49

of γ rays that reach the array surface by the total number of emitted γ rays, independently of the energy they had. The intrinsic efficiency would be then the quotient between the total and the geometric efficiencies.

We can estimate the geometric efficiency. For a source at rest emitting isotropically it is the ratio between the solid angle covered by the detector $(d\Omega)$ and the total solid angle that should be covered to collect all the emitted γ rays (Ω), which is equal to 4π stereo-radians. The solid angle covered by our detector is approximately $\frac{s}{d^2}$, where $\mathbf{s}$ is the detector surface seen by the source and $\mathbf{d}$ is the distance between the detector and the source. All this is shown in the formula 3.2.

$$\epsilon_g = \frac{d\Omega}{\Omega} = \frac{s}{4\pi d^2}\left(= \frac{2.067\ cm^2}{d^2}\ in\ our\ case\right) \qquad (3.2)$$
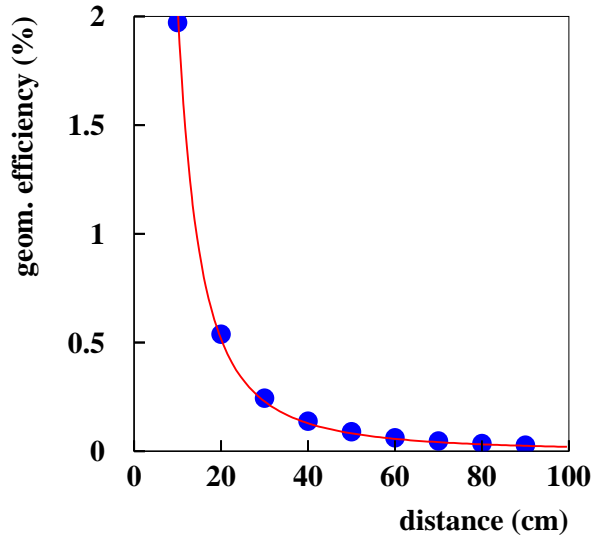

Figure 3.6: *Comparison between the geometric efficiency estimation (line) and the results obtained with the simulation (points), as a function of the distance source-detector.*

We can compare the estimation we have made to the results obtained with the simulation for different distances and for a single NaI crystal of the

Table 3.1: Comparison between the measured and simulated total efficiency dependence with energy

Energy (keV)	Experiment	Simulation
847	0.36 %	0.36 %
898	0.35 %	0.35 %
1238	0.23 %	0.30 %
1836	0.21 %	0.24 %
2598	0.14 %	0.18 %
3243	0.08 %	0.15 %

array (without shieldings). This is shown in the figure 3.6. We can conclude that our estimation is correct and the detectors size and shape do not play an important role in the geometric efficiency dependence with the distance. Coming back to the experiment, the total, geometric and intrinsic efficiencies obtained in each case are presented in the following sections together. Some considerations related to the goodness of the fit between simulation and reality are presented as well.

3.3.1 Radioactive sources at rest

We present the results corresponding to the simulated efficiencies for the sources at rest. The table 3.1 shows the comparison between the total efficiency for the experiment and the simulation. The geometric efficiency of the whole array has been calculated with the simulation and has a value of 1.1 % (remember that for sources at rest emitting isotropically we have a unique geometric efficiency).

The agreement between the simulation and the experiment at low energies is very good.

At higher energies there are some fluctuations mainly due to problems in the fit to the experimental data, specially when the distinction between background and photo-peak was hard to be done (look, for instance, the figure 2.7). Figure 3.7 shows the graphical comparison between measured and simulated total efficiency as a function of the energy.
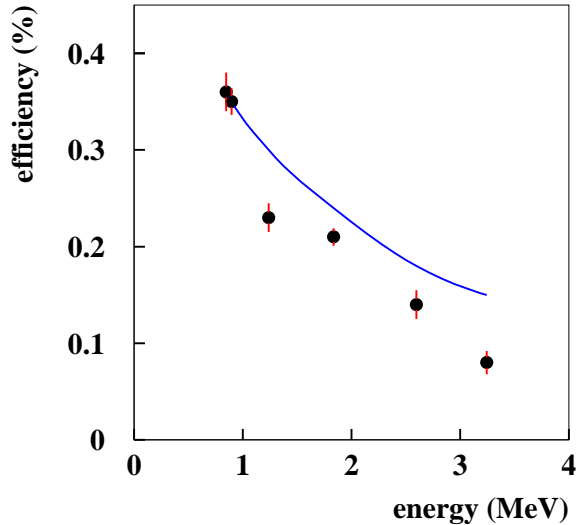
Figure 3.7: *Total efficiency dependence of the whole array with the energy. The line corresponds to the simulation and the dots to the experiment.*

3.3.2 Moving sources

We have checked the simulation for sources at rest with the experimental results. We concluded from the quality of the agreement the validity of our simulation tool. We can then extrapolate the simulation to relativistic moving sources giving γ rays at higher energies and emitted in an angular distribution peaked in the forward direction. The detector simulation overcomes no change when the angular distribution changes and thus its behavior is supposed to be correct. It is possible, then, to predict the values of the efficiencies for the γ rays emitted by some excited moving nuclei produced at the breakup target by considering the simulated setup for the in-beam γ rays (already mentioned before) applied to the specific situation which is going to be simulated by modifying the values of the energies of the emitted γ rays. The estimation of those values is extremely useful for the later analysis of the experiment and is one of the important results of the present work.

The total, geometric and intrinsic simulated efficiencies for some interest-

Table 3.2: Total, geometric and intrinsic efficiency obtained from the simulation for different γ rays emitted by some interesting nuclei produced at the breakup target during the experiment.

Nuclide	Energy (keV)	ϵ_t (%)	ϵ_g (%)	ϵ_i (%)
^7Be	428	2.9	10.9	26.6
^{20}O	1638	0.98	11.6	8.4
^{22}O	3190	0.37	11.9	3.1

ing nuclei produced at the breakup target during the experiment are shown in the table 3.2, were the energy is in keV and corresponds to the already Doppler corrected γ ray energy. The first thing we observe is a decrease in the intrinsic efficiency from one nucleus to the other. This is due to the variation of the total interaction cross-section for the γ rays in NaI as their energy increases (see figure 2.9). We can note that now this decrease is faster (compared with the observed for the case with sources at rest) because the γ rays in this case are seen Doppler shifted to higher energies by the detector (β=0.867). The geometric efficiency is expected to be higher than in the sources at rest because the Doppler effect distorts the isotropic emission of the γ rays to a forward-peaked distribution, increasing the number of γ rays that hit our detector. The small variation observed in the geometric efficiency for the three nuclides in the table 3.2 is explained if we consider that the most energetic γ rays will have a higher probability to pass the shielding and arrive at the detector surface.

In figure 3.8 we show the comparison between the total efficiency obtained with the simulation for radioactive and moving sources.

We can observe than the particular kinematical conditions of moving sources at around 1 GeV/nucleon it is translated in a gain of a factor of 4 to 8 in the total efficiency for the same detector system.

Another point that was already mentioned before in this work is the large reduction in energy resolution experimented for moving sources compared to radioactive sources at rest. The Doppler broadening will be responsible of this poor energy resolution. To give a feeling of this effect, the resolution for a 3 MeV moving source would be of around 30 % compared to the 10 % expected (with our detectors) for radioactive sources at rest emitting gammas at the same energy.
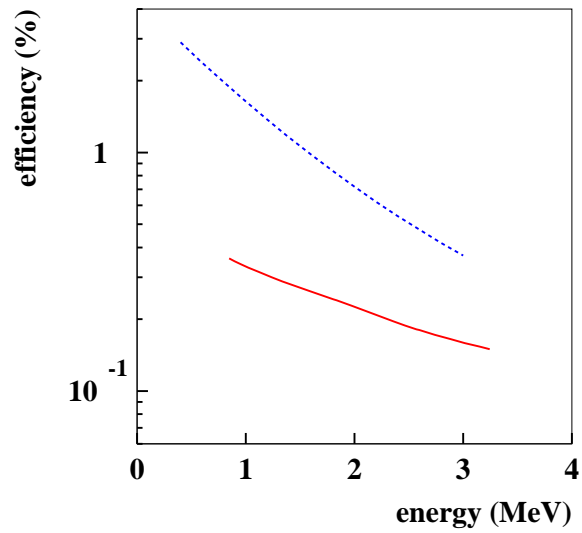
Figure 3.8: *Comparison between the total efficiency obtained with the simulation for radioactive (solid line) and moving sources (dashed line).*

Chapter 4

Possible improvements of the experimental setup

In this chapter we want to focus on two points:

- To describe the deficiencies we find in the analysis of the experiment and the way in which we can minimize them.

- To identify the variables we can change to improve the experimental setup for future experiments.

Detector efficiency and Doppler shift:

For a gamma detector, the intrinsic efficiency (the ability to collect all the γ ray energy) decreases with increasing energy. The main contribution to the photo-peak is the photo-electric effect, where the ejected electron looses all its energy inside the crystal. This interaction is the most probable at low energies (till around 1 MeV). At intermediate energies (from 1 MeV to 5 MeV), the biggest probability is for the Compton effect. In this case, the ejected electron is collected inside the crystal, but the scattered γ ray can either become absorbed or escape if the crystal size is small. When this happens, the γ does not contribute to the photo-peak and in consequence the detection efficiency is small. For higher energy γ rays, multiple Compton scattering helps the scattered γ rays to escape, reducing the detector efficiency more and more. When the pair production effect becomes the most probable interaction in the crystal, the detection efficiency stabilizes or recovers a little (at around 5 MeV). For a detailed description of the different interactions influence on the detection efficiency see reference [26]

From a conceptual point of view there is no difference in the detector efficiency when the γ rays are emitted by a moving source but, due to the Doppler effect, the detector sees them with different energy and this will modify the detection efficiency for the same γ ray energy. In our experiment, they suffer a shift towards higher energies, and consequently we expect a dramatic decrease in the intrinsic efficiency based on the facts exposed in the last paragraph. In the other hand, the Doppler shift enhances the geometric efficiency peaking the emitted γ rays distribution towards the forward direction (see figure 2.8). These two effects govern the total efficiency variation as we will see later.

In our experiment we have to deal with relativistic moving sources that emit γ rays strongly Doppler shifted to very high energies. This makes very difficult to distinguish the γ rays from the background (mainly contributions from different reaction fragments, such as neutrons and charged particles) because the detection efficiency decreases with the energy (see figure 2.7). To improve the total detection efficiency several things can be done: to choose higher efficiency detectors made of high Z and high density materials to improve the photo-fraction, to use bigger detectors in order to avoid that the gamma rays escape without loosing all their energy, to use geometries that increase the geometric efficiency and more. We will treat each one of these possibilities in this chapter.

Doppler broadening:

This phenomenon is due to the uncertainty in the source and γ ray velocity vectors when we do the Doppler correction. The Doppler broadening dependences are shown in the equation 4.1.

$$
\begin{aligned}
\Delta E_{lab} = E\Big(\frac{\beta \, sen\theta_{lab}\sqrt{1-\beta^2}}{(1-\beta cos\theta_{lab})^2} \cdot \Delta\theta_{lab} + \\
\Big(\frac{\beta}{\sqrt{1-\beta^2}(1-\beta cos\theta_{lab})} + \frac{cos\theta_{lab}\sqrt{1-\beta^2}}{(1-\beta cos\theta_{lab})^2}\Big) \cdot \Delta\beta\Big)
\end{aligned}
\tag{4.1}
$$

In this formula ΔE_{lab} is the Doppler broadening, E_{lab} and E the energies of the γ rays in the detector and in the center of mass system, β the velocity of the emitter, θ_{lab} the angular position of the detector, and $\Delta\beta$ and $\Delta\theta_{lab}$ the uncertainty in the velocity and in the angle between the emitter and γ

ray tracks. We observe that the Doppler broadening depends linearly on the γ ray energy. We will try to analyze the different contributions.

The uncertainty due to $\Delta\beta$ can be greatly minimized in our case, because we measure the specific velocity vector of each emitter. With this correction there is still an uncertainty originated by the TOF resolution that we have in our experiment (120-150 ps $\simeq$ $\Delta\beta = 0.0009c$), and an uncertainty introduced by the energy loss suffered by the projectile and the fragment emitter in the different materials. In any case, this contribution to ΔE_{lab} is negligible compared to the one due to the angular uncertainty.

We can also reduce $\Delta\theta_{lab}$, because we know the initial point of the γ ray track (if we suppose that the excited nuclei produced in the breakup reaction decay very fast [22] and we approximate the emission point to the target position). The initial coordinates of the γ ray will be the coordinates of the emitter at the target position given by the tracking detectors (the TPCs).

This is a considerable reduction, but the main Doppler broadening source is the fact that our detectors are not punctual: they cover a finite solid angle viewed from the source, introducing an uncertainty at the end of the emitted γ ray track since is not possible to know which point of the detector hit the gamma. The best way to reduce this effect is to use (really or virtually) smaller detectors as we will see later in this chapter.

The Doppler broadening is strongly linked to the geometric efficiency because both depend directly on the size of the detector. It is very important to find an equilibrium between these two variables that fulfills all the requirements necessary for the experiment. A nice solution to this problematic interdependence is the Add-back procedure: small detectors virtually joined together into a bigger one or a big detector virtually divided into smaller parts. We assign all the energy of the group of small detectors to just one (the first hit) considerably reducing the angular uncertainty. In this way we are in an optimum situation: bigger efficiency and lower Doppler broadening. For a graphical explanation see figure 1.13.

Detector materials:

Even if we were able to completely eliminate the Doppler broadening effect in the energy spectra, the photo-peaks would still have a certain width. As we have discussed in the section 3.2.2 this width is due to the intrinsic en-

ergy resolution of the detector and increases linearly with the energy for high
energy γ rays. The energy resolution is characteristic of the material and de-
pends on the signal produced per amount of radiation in the detector.

Finally, we must look for a good time resolution (linked to the velocity
response of the detector), that is an important characteristic to effectively
reduce the background (mainly neutrons and charged particles), by discrim-
ination of the γ rays peak from other contributions as we have already men-
tioned in section 1.3. In order to choose the right detector we need to look
at the materials characteristics.

4.1 Comparison between different materials

In this section we present different materials that can be used in γ ray spec-
troscopy: inorganic scintillators and semiconductors. The goal is to com-
pare their specific characteristics and to select the best material for in-beam
gamma ray spectroscopy at relativistic energies (around 1 GeV/nucleon).

We are interested mainly on three of their characteristics: energy reso-
lution, time resolution and photo-fraction (directly related to the intrinsic
efficiency). We will look at these characteristics to do the material choice.
Finally, the detector must be exposed to radiation (mainly neutrons and
charged particles coming from the beam) so, if it is possible it would be con-
venient to select one that is resistant against radiation damage, or to use a
pulser to follow the deviations in its behavior.

4.1.1 Inorganic scintillators

In this group we focus on the alkali halides, the fluorides and the oxides,
which are the main inorganic materials used for gamma detection.

The scintillation detector [20, 26] is mainly a scintillator material (in this
case an inorganic scintillator) that emits light when gamma radiation pass
through it and excites the material atoms and molecules. This light is then
transmitted to a photomultiplier where it is converted into a weak current of
photoelectrons. This current is greatly amplified in the device before passing
to the electronics.

To obtain a good energy resolution, we have to choose detectors with a high signal per amount of radiation absorbed in the crystal. This characteristic depends on the material light yield, and on the photomultiplier gain for the light emitted by the scintillator.

The time resolution is directly related to the decay constant of the scintillator light emission. This light emission is given, in first approximation [20], by the formula 4.2, where N is the number of photons emitted at time t, N_0 the total number of photons emitted, and τ_d the decay constant.

$$N = \frac{N_0}{\tau_d} \cdot e^{-\frac{t}{\tau_d}} \tag{4.2}$$

In the table 4.1 we show the main characteristics for different scintillation materials. The material that better represents an equilibrium between all the characteristics we need in order to accomplish our experimental requirements is the NaI(Tl), presenting relatively good energy and time resolution and a convenient photo-fraction.

Sometimes it is difficult to distinguish between the different particles leaving their energy in the material. In this case it would be interesting to have a good time resolution to correctly select only the γ rays. This can be achieved with a fast response scintillator with different decay constants, like the BaF_2. This material presents a better photo-fraction, although it has the disadvantage of a poor energy resolution. An intermediate solution between the NaI(Tl) and the BaF_2 is the CsI(Na).

4.1.2 Semiconductors

A semiconductor detector operates in the following way [20, 26] : when an ionizing radiation enters the material, it normally creates electron-hole pairs which are then collected by an electric field, and give rise to an electric pulse proportional to the energy of the incident radiation (the number of created pairs increases with the radiation energy).

Among the advantages of these detectors are the low energies required to generate pairs (which causes a better energy resolution) and their fast response times. The main disadvantage is that semiconductors require low temperatures to work properly, are available only in small sizes and their price is high.

Table 4.1: Comparison between different scintillators characteristics [25].

material	density (g/cm^3)	light yield (% NaI(Tl))	photo-electron yield (% NaI(Tl))	τ_d (ns)
NaI(Tl)	3.67	100	100	230
CsI(Tl)	4.51	137-147	45	1000
CsI(Na)	4.51	100-116	85	630
CsF	4.64	5	5-7	3-5
BaF$_2$	4.88	17 (slow)	16 (slow)	630 (slow)
		7 (fast)	5 (fast)	0.6-0.8 (fast)
GSO(Ce)	6.71	21-26	20	60
BGO	7.13	21-26	15-20	300
CdWO$_4$	7.9	31-39	25-30	20000-5000

The semiconductors fulfill two of the requirements to solve the experiment problems: good energy and time resolution. But their low photo-fraction results in a poor detection efficiency (specially at high energies). This is a very important fact that depending on the experimental conditions may condition the election between scintillator or semiconductor detectors for a γ ray measurement.

The tendency at low or intermediate energies is to use germanium detectors to perform on-line γ ray spectroscopy, but in our case (sources at around 1 GeV/nucleon), the Doppler broadening is at the origin of a poor energy resolution and the Doppler shift makes the γ rays energies higher and it is at the origin of the dramatic decrease in intrinsic resolution.

For this reason it is not worthy to select a very good energy resolution detector if the Doppler broadening is going to reduce this resolution, specially if the detector has a poor detection efficiency for the high energy γ rays that are emitted by the moving fragments. This is why we used individual NaI(Tl) crystals in the experiment instead of other materials, such as germaniums.

4.2 Geometry optimization

In this section we will try to analyze the effect the detector geometry has on the main difficulties we face in our experimental setup (efficiency and Doppler broadening) in order to propose an optimization for future experiments. A simulation is a very useful tool for this purpose, since it allows us to easily change the different parameters involved in the setup. The results obtained in the moving sources case for different positions (angle and distance) and sizes of an individual NaI crystal taken from our array are treated in the next subsections.

4.2.1 Polar angle between the beam axis and the detector

In order to find the best angular position to place our array we proceed in the following way:

We define the "optimum" angular position as the one that provides the highest total detection efficiency. To do the optimization we divide the total detection efficiency concept into the geometric and intrinsic components. We maximize the geometric efficiency of the detector if we place the detector in the maximum of the emitted γ rays angular distribution (figure 4.1 left, top). At the same time, the best intrinsic efficiency is achieved for the smallest Doppler shifted γ rays (figure 4.1 left, bottom). We want to signal that all the examples presented correspond to a beam velocity of 0.8667c. The angle of 0.0 radians corresponds to the beam direction.

The first approximation to the polar angle optimization is to use a weighted histogram method to decide which is the "optimum" angle considering the main dependences described above. This is done in the figure 4.1 (right), where the angular distribution is multiplied by the inverse of the Doppler shift angular dependence histogram, channel by channel. In this way the maximum for the distribution results at around 0.52 radians.

But this is maybe a very simple way to attack the problem. If we want to obtain the total efficiency dependence on the angular position in a realistic way, we need a new simulation to include the detector behavior together with the angular dependence.

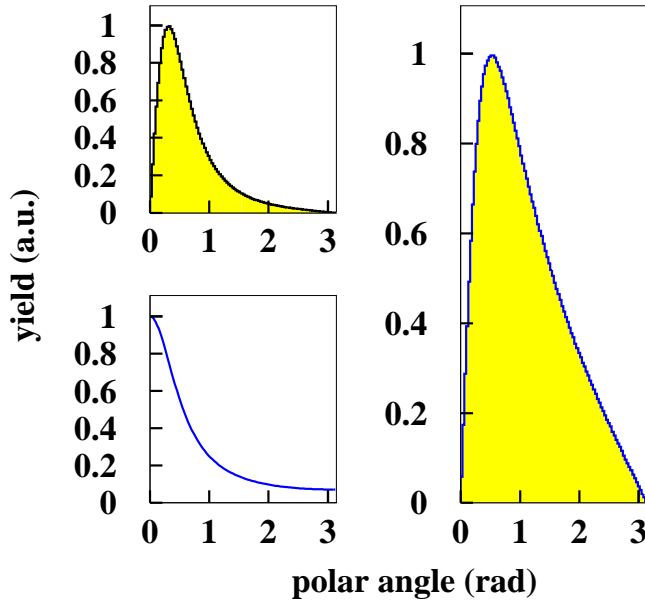We simulated for this purpose a geometry consisting of 19 NaI detectors

Figure 4.1: *Combined effect of the emitted γ rays angular distribution (left,
top) and the Doppler shift dependence with angle (left, bottom) to generate
the Doppler shift weighted angular distribution (right). All the histograms
have been normalized to 1 in their maxima.*

(of identical characteristics to the ones used in our array). The simulation
included only the crystals, without shieldings. They were located with a ra-
dial disposition at different polar angles (from 0 to π radians). The distance
between each detector surface and the source was 50 cm. (see figure 4.2).
Due to the existing cylindric symmetry, the information obtained is extensi-
ble to all the possible azimuthal angles.

We studied the total efficiency variation with the angular position of the
detector in the ring for a pack of γ rays (Energies: 0.6, 1.1, 1.6, 2.1, 2.6,
3.1, 3.6 MeV. Branching ratios: all equal to 1) that are emitted by sources
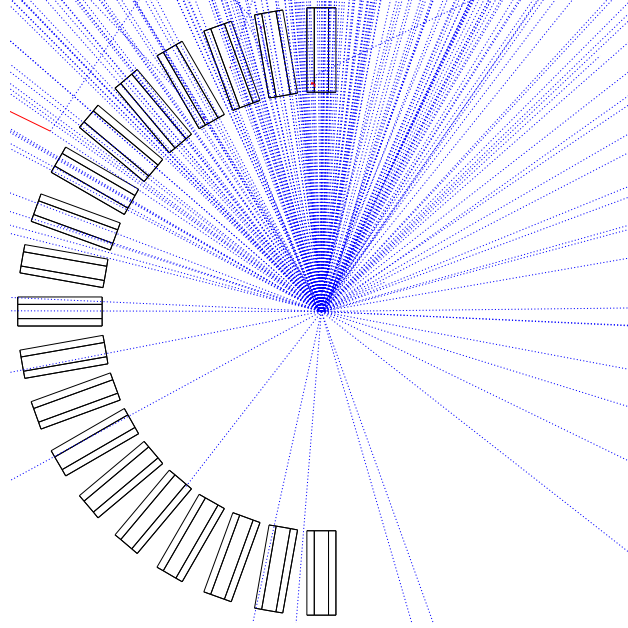moving at 0.8667c.

Figure 4.2: *Schematic view of the simulated setup to study the efficiency and Doppler broadening dependence on the angular position. The distance between the source and the detector surface is 50 cm.*

The results obtained in our particular case are shown in the figure 4.3. As expected, the efficiency is lower for the higher energy γ rays. The shapes of the different curves are not just different by a constant multiplying factor. The election of the angular position is very important for low energy γ rays, but for the high energy ones the variation in the detection efficiency becomes less dramatic. We observe that for all the γ rays, the detection efficiency drops very quickly to zero when the polar angle is bigger than $\frac{\pi}{2}$ rad.

Although the total detection efficiency optimization is the fundamental reason for this chapter we cannot forget the Doppler broadening effect (figure 4.4 shows its angular dependence compared to the intrinsic resolution angular dependence of a typical NaI crystal of the array), because if the energy resolution results too bad it can be very difficult to distinguish the peaks from the background. We observe that at those energies, the Doppler broadening dominates for almost all the angular range and it would be the main reason of the NaI detector energy resolution.

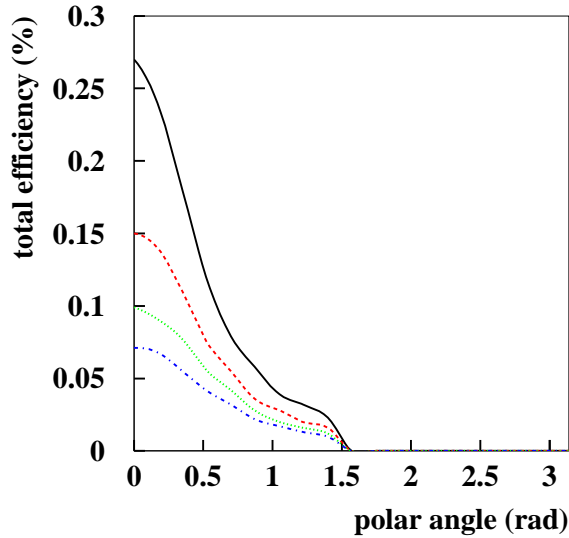We must take into account the angular dependence of both problems (to-

Figure 4.3: *Simulated total efficiency response with energy for different NaI
crystals located at different angles and emitting γ rays energies. The solid,
dashed, dotted and dashed-dotted lines are for 0.6, 1.1, 1.6 and 2.0 MeV γ
rays respectively for a β= 0.8667 c.*

tal efficiency and Doppler broadening) to find the best place for our detector.
To find the optimum angular position we use the weighted histogram method.
The two variables are now the total efficiency and the Doppler broadening
effect. The decision histogram that results is shown in the figure 4.5, and the
best polar angle to position our detector is zero radians. This is logical, since
the detection efficiency is maximum and the Doppler broadening is minimum
at this value. In practice, we cannot choose this polar angle in the experiment
because the beam passes through it and would damage the detector. If we
look at the decision histogram we can see that the other angular positions till
$\frac{\pi}{2}$ radians are roughly equivalent with the weighting we have done. We can
choose, for instance, a polar angle of 0.17 radians between all the possible
elections to maximize the efficiency.

In the experiment the average polar angle of the array was 0.3 rad. Even
if we will keep the 0.17 values for the rest of the simulation, we conclude
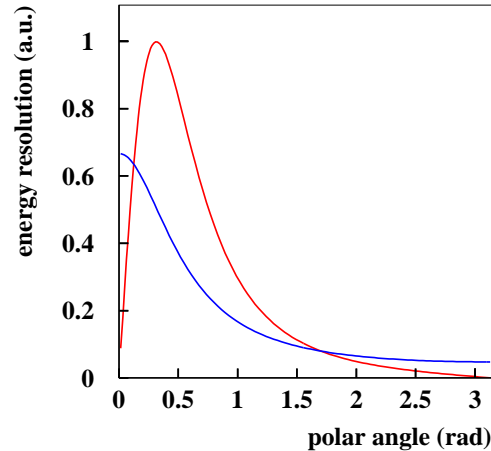
Figure 4.4: *Doppler broadening angular dependence (grey line) compared to the intrinsic resolution angular dependence of a typical NaI crystal (black line). The results have been obtained for a typical NaI crystal of the array located at a distance of 50 cm (between the detector surface and the target). The units in the y axis are set in such a way that the Doppler broadening is normalized to one in their maxima.*

that the polar angle of the NaI array is the optimum for detection of γ- rays emitted by moving sources at 1 GeV/nucleon.

4.2.2 Distance between the target and the detector

We want to obtain the maximum possible efficiency without loosing too much resolution by Doppler broadening. These two conditions constrain the distance value between the source and the detector. If we run the simulation for different distances, setting the beam velocity to 0.8667c (typical value for the fragment velocity in our experiment) and the position polar angle of the detector with respect to the beam axis to 0.17 radians (value selected in the last subsection) we obtain the total efficiency distance dependence (figure 4.6, left) and the Doppler broadening distance dependence (figure 4.6, right), in this particular case, for a 2.1 MeV γ ray. The Doppler broadening distance dependence with the distance source-detector is shown in figure 4.6
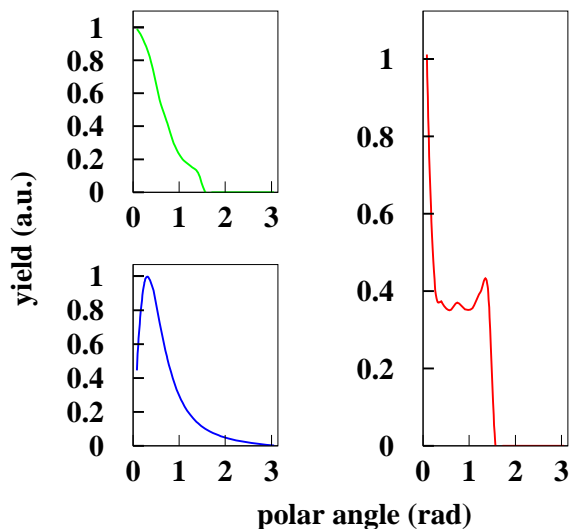
Figure 4.5: *The total efficiency of the detector for a 2.1 MeV γ ray (left, top) is combined with the Doppler broadening (left, bottom) to obtain the decision histogram to find the best angular position for the detector (right). All the histograms have been normalized to 1 in their maximum.*

left and it is compared to the intrinsic energy resolution for a typical NaI crystal of the array. We observe that the Doppler broadening dominates the energy resolution for small distance source-detector

To deduce the most satisfactory distance between the target and the detector for the constrains we have, we must decide the importance we give to the minimization of the efficiency problem (figure 4.6, left) and the importance we give to the minimization of the Doppler broadening one (figure 4.6, right). This is accomplished, in a similar way as for the angular position case. The decision histogram shows the optimum position for the detector (the point where the curve is maximum) for a distance between target and detector around 10 centimeters, but it is impossible to set the detector at this position since there is a TPC there. We then choose a distance of 30 cm. to leave space for this tracking detector.
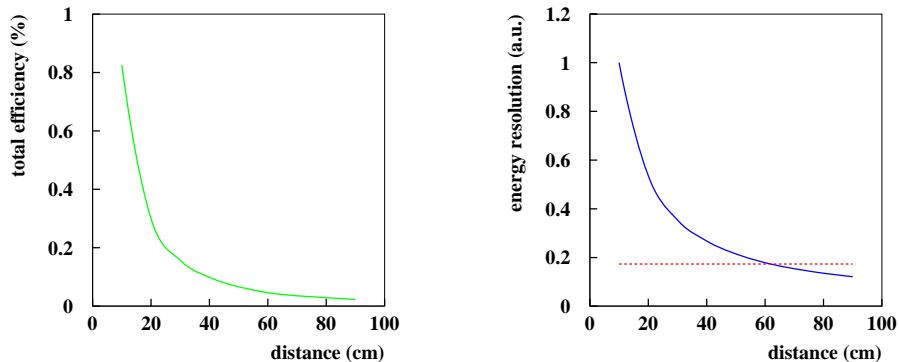
Figure 4.6: *Left: variation in the total efficiency of an individual NaI crystal of the array for different distances detector-target. Right: Doppler broadening dependence on the distance between the target and the detector (solid line). The energy resolution from the Doppler broadening is compared to the intrinsic resolution of a typical NaI crystal of the array (dashed line). The units in the y axis are set to normalize to 1 the Doppler broadening in its maximum. For both figures, the polar angle between the detector position and the beam axis is 0.17 radians, the beam velocity is 0.8667c and the γ ray energy is 2.1 MeV.*

In fact we know that at this distance we will have a very poor energy resolution (figure 4.6 left) and we can conclude that the distance of 80 cm chosen in the experiment is a very good compromise solution because it optimizes the energy resolution in despite of an acceptable reduction of the total efficiency.

4.2.3 Detector size

For a fixed position, the detector size is strongly related to the geometric efficiency and it also influences the intrinsic efficiency through the photofraction. As a consequence of this, by increasing the size we can considerably enhance the detection efficiency. For moving sources, the detector size is also linked to the Doppler broadening effect and its influence must be considered. In this section we are going to study the influence of the detector size on these two problems (efficiency and Doppler broadening) as we have already done for the detector position. We consider a moving source, with a velocity
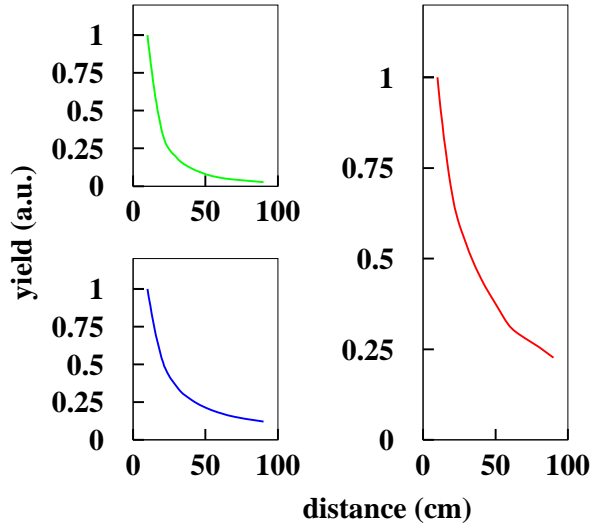
Figure 4.7: *The total efficiency of the detector (located at an angular position of 0.17 radians) for a 2.1 MeV γ ray (left, top) is combined with the Doppler broadening (left, bottom) to obtain the decision histogram to find the best distance between the target and the detector (right). All the histograms have been normalized to 1 in their maximum.*

of 0.8667c, emitting a 2.1 MeV γ ray and only one individual crystal of our array. The crystal is located at a distance of 30 cm. from the target. Its angular position is 0.17 radians.

In the figure 4.8 (left) we present the results obtained with our simulation for different crystal sizes. In our example, the size changes as a whole, maintaining the crystal proportions. As can be seen, the total efficiency increases very fast with increasing size. In the figure 4.8 (right) we show the Doppler broadening variation for different crystal sizes compared to the intrinsic resolution of a typical NaI crystal of the array. The Doppler broadening increases linearly with the detector size. We observe that at those energies the Doppler broadening dominates for detector sizes starting with a factor 2 smaller than the NaI detectors used in the experiment.
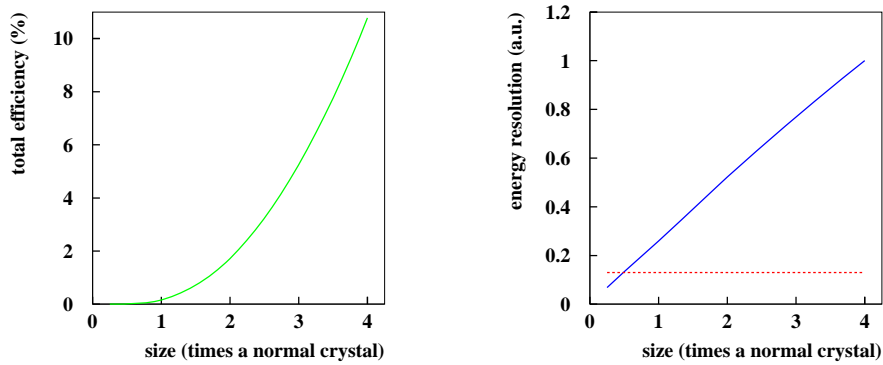
Figure 4.8: *Left: total efficiency dependence on the NaI crystal size. The size is N times a normal crystal used in the experiment. Right: Doppler broadening dependence on the NaI crystal size (solid line). The energy resolution from the Doppler broadening is compared to the intrinsic energy resolution for a typical NaI crystal of the array (dashed line). The y axis units have normalized to 1 for the Doppler broadening. Both figures correspond to a beam velocity of 0.8667c and a fixed position of the detector (0.17 radians and 30 cm. distance between the detector surface and the target). The γ ray energy is 2.1 MeV.*

To choose the optimum size for our detector we must weight both contributions in the same way we did for the position analysis. In the resulting histogram (figure 4.9) we must choose the point where the curve is maximum. This happens for the maximum size of the crystal, and is a logical conclusion if we notice that the total efficiency increases greatly with the crystal sized compared to the linear dependence of the Doppler broadening. In any case if we select such a huge detector we will suffer for a extremely poor energy resolution.

All these considerations allow us to conclude that the parameters chosen for the NaI array used in the experiment were close to the optimum ones for this kind of detectors and at those particular energies. Future minor improvements for such an array could come from the used of bigger number of detectors to cover a larger solid angle improving the geometric efficiency, with smaller sizes to reduce the Doppler broadening and improving the energy resolution.
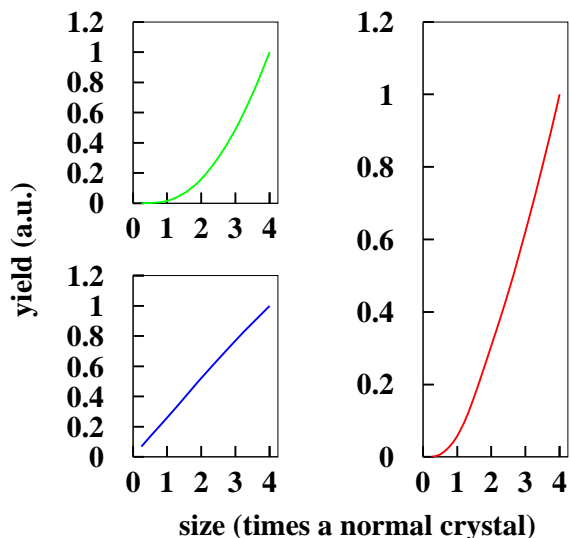
Figure 4.9: *The total efficiency of the detector (located at a polar angle of 0.17 radians and 30 cm. distance between the detector surface and the target) for a 2.1 MeV γ ray (left, top) is combined with the Doppler broadening (left, bottom) to obtain the decision histogram to find the best size for the detector (right). All the histograms have been normalized to 1.*

4.3   Examples with real detectors

As we have seen all the long this work the NaI array used presents strong experimental restrictions. Even though the total efficiency of our NaI improved for the case of moving sources emitting γ- rays, the absolute efficiency remains very low. This would means that our experiments would suffer from poor statistics that would difficult the results interpretation. We want in this section to study the efficiency expected with other existing γ- ray detectors in GSI to check the performances they could provided.

In this section we present the results obtained with our simulation applied

to different real detectors geometries (Super Segmented Clover detector, CsI array detector) and we compare them with the values for the total, geometric and intrinsic efficiencies at rest and for moving sources cases for the NaI array.

From these comparisons we will extract some conclusions about the preferences to choose one or other of the presented detectors for the in-beam γ ray spectroscopy part in future experiments.

4.3.1   One(or more) Super Clover(s)

We start the study of alternative detectors with the Super Segmented Clover (Super Clover) [27].

The Super Clover has been developed at GSI in a collaboration with the company Eurisys, Strasbourg. It consists of four coaxial Germanium detectors of 14 cm. length and 7 cm. diameter enabling an optimal arrangement with respect to efficiency and spectrometer response. To further improve the Doppler correction capability, the detector elements are electrically segmented in radial quarters and these radial quarters are then conveniently grouped in 9 different sub-detectors (see figure 4.10) for explanation.

Since the sub-detectors are of different size, as it is shown in figure 4.10, the detection efficiency and Doppler broadening will be also different depending on the particular sub-detector considered.

The main deficiency of this detector comes from the small solid angle covered. To improve the total detection efficiency, several Super Clover detectors can be used to cover a bigger solid angle thus increase the geometric efficiency.

The main contribution to the energy resolution is clearly the one due to the Doppler broadening because the intrinsic energy resolution is in this case very small (the material is a semiconductor and semiconductors have a very good intrinsic energy resolution).

The Super Clover was located in our simulation at a mean polar angle of 0.3 radians and the distance between the source and the detector surface is 37.5 cm.

If we compare the values obtained for the total efficiency with radioactive sources at rest (table 4.2) with the values obtained in the NaI array case
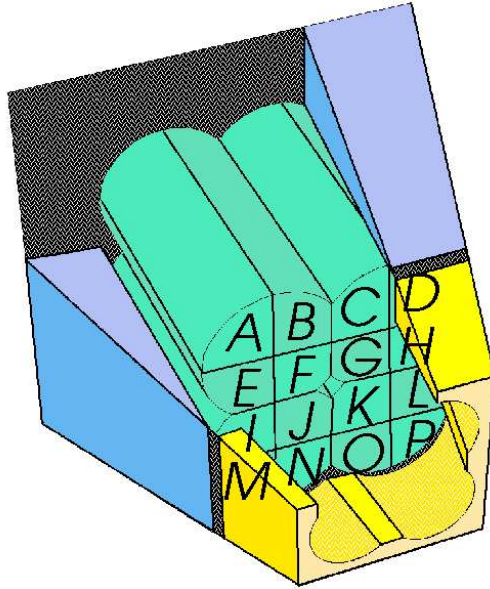
Figure 4.10: *View of the Super Segmented Clover Detector developed at GSI consisting of four large, four-fold segmented Germanium crystals in a BGO Compton suppression shield. The scintillator in front is used as an active collimator. In the simulation the Super Clover was considered to be formed by 9 independent germanium detectors: 1=a, 2=b+c, 3=d, 4=e+i, 5=f+g+j+k, 6=h+l, 7=m, 8=n+o, 9=p (this is the same arrangement that is done in the reality).*

(table 2.1) we can see that the total efficiency is lower for the Super Clover. Taking into account that the geometric efficiency for the Super Clover setup is 0.39 % and the geometric efficiency for the NaI array setup is 1.1 %, is clear that is the geometric efficiency the responsible of the main difference between both configurations.

In the case of γ rays emitted by sources moving with velocity 0.8667c (table 4.3), due to the change in the γ ray angular emission from isotropic to peaked in the forward direction as a consequence of the Doppler effect, there is an enhancement in the geometric efficiency of the Super Clover. The Doppler effect also causes a reduction of the intrinsic efficiencies, and the final effect over the total efficiencies is a moderate increase. The total efficiencies obtained for the Super Clover with this configuration are one third of the efficiencies obtained for the NaI array. That means that with three Super Clover detectors located at different azimuthal angles we end up with

Table 4.2: Total efficiency obtained from the simulation of the main γ rays emitted by the ^{88}Y and ^{56}Co sources at rest with respect to the detector.

Energy (keV)	ϵ_t (%)
847	0.099
898	0.096
1238	0.077
1836	0.062
2598	0.046
3243	0.039

Table 4.3: Total, geometric and intrinsic efficiency obtained from the simulation for different γ rays emitted by some interesting nuclei produced at the breakup target during the experiment.

Nuclide	Energy (keV)	ϵ_t (%)	ϵ_g (%)	ϵ_i (%)
^7Be	428	1.00	5.35	18.69
^{20}O	1638	0.33	5.35	6.17
^{22}O	3190	0.11	5.35	2.06

the same total efficiency as in the NaI case.

In the figure 4.11 we show the comparison between the total efficiency obtained with the simulation for radioactive and moving sources for the Super Clover detector.

If we compare the intrinsic energy resolution for one Super Clover detector (0.3 % at 1.3 MeV), with the approximate value of the Doppler broadening obtained with this setup (34 %) we observe than we are not taking the best profit of the exceptional energy resolution characteristic of semiconductor detectors, and at the same time we are loosing in intrinsic efficiency. For this reason, if we want to obtain the sharp peaks the Super Clover is able to provide, we have to reduce the Doppler broadening. This reduction can be effectuated by extra-dividing the Super Clover.
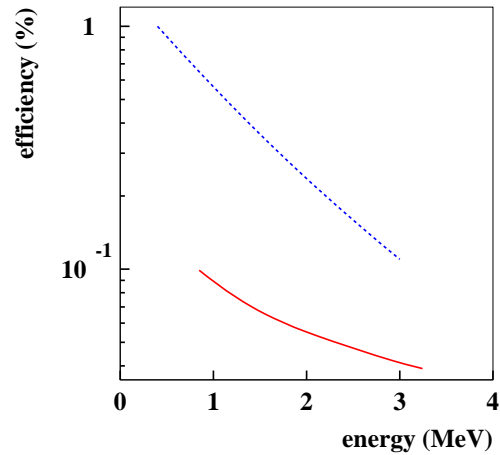
Figure 4.11: *Comparison between the total efficiency obtained with the simulation for radioactive (solid line) and moving sources (dashed line) for the Super Clover detector.*

4.3.2   Virtually divided Super Clover(s)

A new experimental technique is going on in the *gamma*-spectroscopy community and in particular in GSI to extra divide the normal Super Segmented Clover detector in a virtual way. The technique is called "pulse shape analysis". It consists in to "divide" each one of the Germanium quarters into 9 subparts, so we end up with 144 individual detectors, which provide a very high granularity that considerably diminishes the Doppler broadening effect. At the same time, this semiconductor detector, with very high energy resolution, makes this device very appropriate for precision in-beam γ ray spectroscopy. In the same way as was discussed for standard Super Clover detectors, we can increase the total detection efficiency by using several detectors to cover a bigger solid angle.

The detector position in the simulation is the same considered in the last subsection (for the standard Super Clover detector case). With this configuration we obtain, for the total efficiency, the values presented in table 4.4 for radioactive sources at rest emitting at the target position. The interesting point is that now (with the actual configuration) the Doppler broadening

Table 4.4: Total efficiency obtained from the simulation of the main γ rays emitted by the ^{88}Y and ^{56}Co sources at rest with respect to the detector.

Energy (keV)	ϵ_t (%)
847	0.023
898	0.022
1238	0.016
1836	0.010
2598	0.0066
3243	0.0048

Table 4.5: Total, geometric and intrinsic efficiency obtained from the simulation for different γ rays emitted by some interesting nuclei produced at the breakup target during the experiment.

Nuclide	Energy (keV)	ϵ_t (%)	ϵ_g (%)	ϵ_i (%)
^7Be	428	0.21	5.24	4.01
^{20}O	1638	0.035	5.24	0.67
^{22}O	3190	0.0075	5.34	0.14

is only 11.3 %, although better values can be obtained with other detector positions. In this way we can obtain a very interesting configuration if we put several extra-divided Super Clover detectors.

In this case the total efficiency is even lower than in the normal Super Clover configuration. Being the geometric efficiency the same (0.39 %) because the detector is the same, we must look for the source of the difference in the intrinsic efficiency part: for the present configuration we have divided each one of the individual readout parts in the normal Super Clover into 9 subparts (each one of these subparts is now an individual detector in the acquisition. We have 9 times more detectors, each one 9 times smaller). This has as main consequence a higher probability for the γ ray inside a detector to escape from it due to the smaller detector size.

If a γ ray escapes, it does not contribute to the photo-peak. In fact, the probability of a γ ray energy to spread and be collected in different neighbor detectors is very high. This diminishes the photo-fraction, so, the intrinsic efficiency (and the total one, for the same geometric efficiency) will be lower.
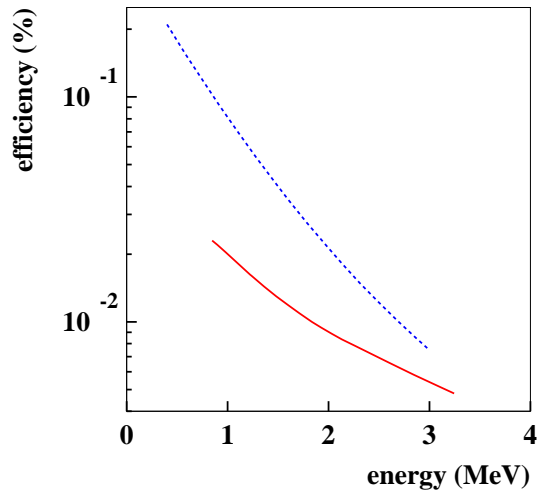
Figure 4.12: *Comparison between the total efficiency obtained with the simulation for radioactive (solid line) and moving sources (dashed line) for the extra-divided Super Clover detector.*

The total, geometric and intrinsic efficiencies obtained with the simulation with moving sources at a velocity of 0.8667c are shown in the table 4.5. Here the values are even lower than in the Standard Super Clover case (the photo-fraction is lower because the size per sub-detector is smaller). Is the prize we have to pay in order to improve the energy resolution.

In the figure 4.12 we show the comparison between the total efficiency obtained with the simulation for radioactive and moving sources for the extra-divided Super Clover detector.

There is a possibility to recover the photo-fraction lost, by using the Add-back procedure. With this method is possible to obtain efficiencies of the order of the ones obtained for the Standard Super Clover, without loosing in energy resolution.

The extra-divided Super Clover detector in combination with the Add-

back procedure is a good election when a high energy resolution and a not too bad total detection efficiency is required.

4.3.3 CsI crystals geometry

The last detector we are going to consider is an array of CsI crystals [28] specially developed to be used for in-beam γ ray spectroscopy at relativistic energies experiments at the GSI. This new detector has been successfully tested with secondary beams of ^{23}O at around 400 keV/nucleon [29] . It has a cylindric geometry and has a hole to let the beam to pass through it. The length of the cilinder is 30 cm. The inner radius is 4.83 cm and the outer one, 19.3 cm. The crystal segmentation has been chosen to minimize the Doppler broadening effect. There are two kinds of segmentations, following the polar and the azimuthal angles. The azimuthal segmentation divides the array into 12 equal parts. The polar segmentation also divides the detector in 12 parts, and it is optimized to minimize the Doppler broadening (the sectors are narrower at higher polar angles).
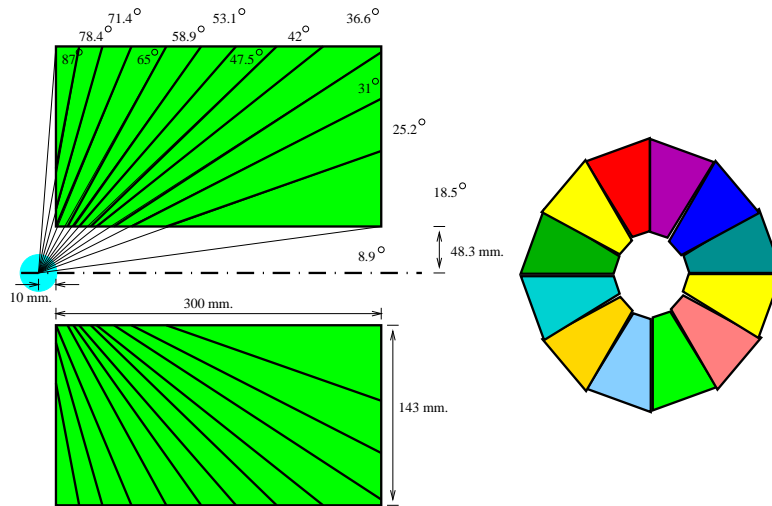

Figure 4.13: *Technical specifications for the CsI detector. The target is located at the center of the point on the left of the figure. The detector presents two kinds of segmentations (polar and azimuthal). It can be seen that the detector segmentation in the polar angle is optimized to minimize the Doppler broadening angular dependence (narrower sectors at higher polar angles).*

Table 4.6: Total efficiency obtained from the simulation of the main γ rays emitted by the ^{88}Y and ^{56}Co sources at rest with respect to the detector.

Energy (keV)	ϵ_t (%)
847	14.84
898	14.09
1238	11.07
1836	8.34
2598	5.59
3243	4.44

Table 4.7: Total, geometric and intrinsic efficiency obtained from the simulation for different γ rays emitted by some interesting nuclei produced at the breakup target during the experiment.

Nuclide	Energy (keV)	ϵ_t (%)	ϵ_g (%)	ϵ_i (%)
^7Be	428	33.29	84.09	39.59
^{20}O	1638	11.82	84.09	14.06
^{22}O	3190	5.54	84.09	6.59

The CsI array detector has been built to be placed very close to the secondary target. In our simulation it is located at 1 cm. away from the target position, as is shown in figure 4.13.

The values obtained for the total efficiency at different energies for radioactive sources at rest are the best obtained values for all the considered detectors (see table 4.6). The really high value for the geometric efficiency of this detector (47.5 %) is the reason for the good results obtained. The intrinsic efficiency is also higher due to the larger size of the CsI sectors and due to the larger Z value and density (factors that increase the photo-fraction) of the CsI with respect to the Germanium or to the NaI.

As expected from the values obtained with radioactive sources at rest, the total, geometric and intrinsic efficiencies for γ rays emitted by sources moving at a velocity of 0.8667c (see table 4.7) are quite high. In fact, they are the highest, for all the presented detectors. This implies that the CsI results a very good detector for doing in-beam γ ray spectroscopy at relativistic energies when the total detection efficiency is the crucial magnitude.
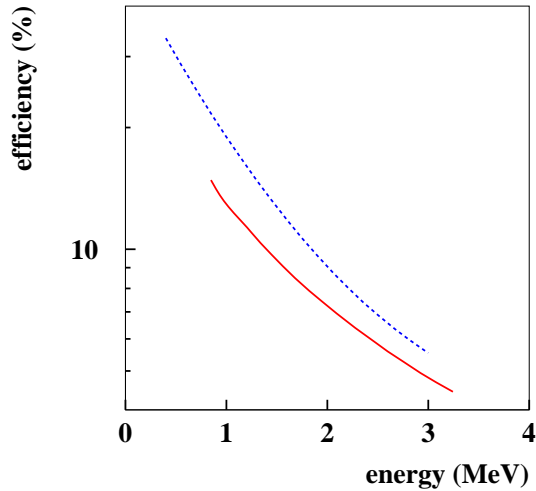
Figure 4.14: *Comparison between the total efficiency obtained with the simulation for radioactive (solid line) and moving sources (dashed line) for the CsI detector.*

In the figure 4.14 we show the comparison between the total efficiency obtained with the simulation for radioactive and moving sources for the CsI detector.

4.4 Results inter-comparison

4.4.1 Total efficiency

We will try to present all the information related to the total efficiency obtained with the simulation in the moving sources case for the different detectors considered in all this work (see figure 4.15). The numerical values obtained for the total efficiency are given in the previous section. We observe that:
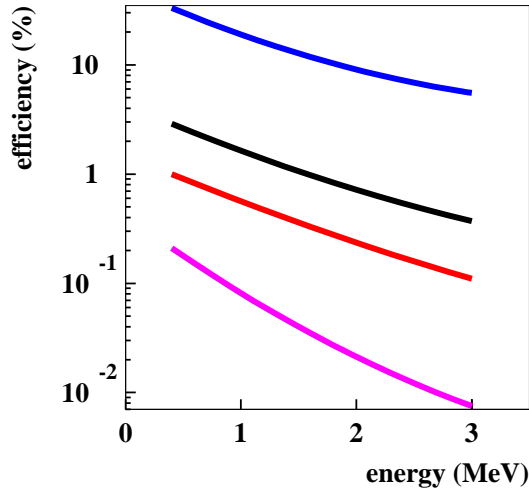
Figure 4.15: *Comparison between the total efficiency obtained with the simulation for moving sources for the detectors studied in this work (from top to bottom: CsI array, NaI array, Super Clover with normal segmentation, Super Clover extra-segmented in the virtual way).*

- With approximately three Super Clover detectors segmented in the normal way we can obtain a total efficiency close to the NaI array one. The question that arises is if the possible gain in energy resolution justifies the more complex (and expensive) setup we would need for these detectors. For the Super Clover extra-segmented in the virtual way we can restore the total efficiency value to the one obtained for the normal Super Clover case using the add-back treatment.

- The CsI array appears to be the best election if we are looking for a high efficiency detector to perform in-beam γ ray spectroscopy at relativistic energies.

4.4.2 Energy resolution

We will try to compare the energy resolution caused by the Doppler broadening on the different simulations together with the intrinsic energy resolution

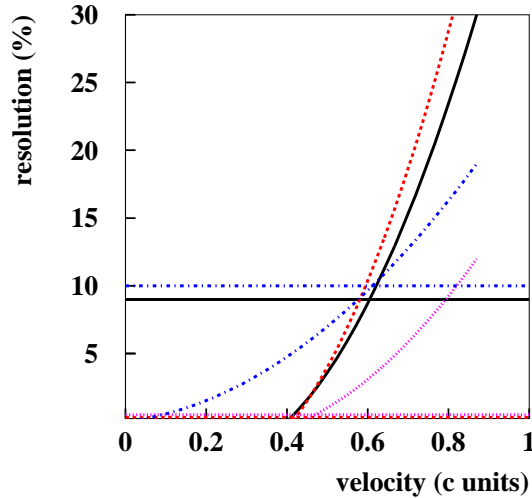corresponding to them (figure 4.16). The main conclusions are:

Figure 4.16: *Comparison between the two components of the observed energy resolution: Doppler broadening and intrinsic resolution (horizontal line) obtained with the simulation for moving sources for all the detectors studied in this work (solid line: NaI array, dashed line: Super Clover with normal segmentation, dotted line: Super Clover with virtual segmentation, and dashed-dotted line: CsI array). The data have been obtained for a γ ray of around 1.6 MeV emitted from a source moving at different velocities.*

- The Super Clover detector segmented in a normal way is not a good election at all (as it is simulated). It not only has a very low detection efficiency: the energy resolution is even worse than NaI array's (≈35 % for E_γ=1.6 MeV). This is of course due to the requirement to place the detector at around 40 cm from the target position (compared to the 80 cm for the NaI array) in order to obtain a total efficiency of the same order as the one observed with our NaI. We could observe that the extremely good intrinsic resolution of the detector (less than 0.5 %) is completely erased by the big Doppler broadening suffered with this geometry.

- The Super Clover extra-segmented in a virtual way is certainly the one with the best energy resolution of all the considered ($\approx$12 % for E$_\gamma$=1.6 MeV). With the help of the add-back procedure it is possible to restore the total efficiency to a value that makes possible using this detector to obtain "good" energy resolution spectra. The energy resolution could improve if we locate our Super Clover at 80 cm from the target. In this case we will improve the energy resolution ($\approx$3 %) but we will need 12 Super Clover detectors to obtain a total efficiency similar to the one obtained with the NaI array. Even in this case we are "destroying" the excellent energy resolution of the Super Clover with the big Doppler broadening related to this particular case.

- The CsI detector has a relatively good energy resolution ($\approx$19 % for E$_\gamma$=1.6 MeV), and at velocities of the order of 0.867c the Doppler broadening and the intrinsic energy resolution are of the same order ($\approx$10 %), what means that this detector optimizes very well its resources to adjust to in-beam γ ray spectroscopy at relativistic energies.

0

Conclusions

We have presented in this work the interest of using in-beam γ-ray spectroscopy at relativistic energies as an alternative to study the nuclear structure of very exotic nuclei,

We have analyzed in detail the new experimental conditions that we would encounter if we use this technique under the kinematical conditions particular to the relativistic energies.

All the experimental work presented in this rapport corresponds to an experiment that we performed at the FRS in GSI. A description, calibration and main physical quantities related to the used detectors and necessary for the completeness of this work, in particular for tracking and particle identification have been presented. We have then centered our attention on the in-beam γ ray spectroscopy part.

For γ detection we used a NaI crystals array placed in an optimum position to get the maximum of the angular distribution of the emitted γ rays (strongly peaked in the forward direction due to the Doppler shift) and trying to minimize the "poor" energy resolution caused by a high Doppler broadening effect (mean distance between the detector surface and the target around 80 cm). In fact, we can give an estimation of the Doppler broadening: 30 %. This value is considerably higher than the intrinsic energy resolution of a typical NaI scintillator at 1330 keV (6 %). The big contribution of Doppler broadening effects to the final energy resolution justifies the use of scintillators (with medium intrinsic energy resolution) instead of semiconductors (with extremely good intrinsic energy resolution).
We have obtained experimentally and then from a GEANT simulation the efficiency of our NaI array for radioactive sources at rest emitting γ rays at different energies. After checking the quality of our simulation, we have obtained from it the efficiency corresponding to the realistic conditions that were present in the experiment: fragments moving at $\beta = 0.8667c$ and emitting γ-rays strongly Doppler shifted.

The final discussions are dedicated to the analysis of the important variables to take into account for future experiments in order to improve the experimental setup: the total detection efficiency, the Doppler broadening effect on the energy resolution, and the time resolution of the detector. All these factors may difficult the task of distinguishing the γ-peaks from the background in different ways:

- A low total detection efficiency decreases the photo-fraction, and the ratio signal-background.

- A high Doppler broadening reduces the energy resolution and broadens the photo-peaks. If the photo-peaks are too broad, they will disappear in the background.

- Finally, if the time resolution is not good enough to allow us to distinguish between the different particles that arrive at our γ detectors in order to select just the γ rays, we will have a strong background due to reaction residues (coming from the target) such as neutrons and charged particles, which difficult the separation of the photo-peaks.

As general conclusion we can say that the detector material, size and position **must be chosen depending on the experiment particularities**: beam size, angular divergence and velocity, position of the γ ray detectors, amount and type of background we have (in order to discriminate the γ rays from other particles in the time spectra), possibility to adapt the shape and size of detectors, stability in the energy calibration, etc. In order to study the best configuration to use in an experiment of these characteristics we have performed a complete simulation which allows us to easily change the setup (detector material, geometry, position) and compare different possibilities.

If the goal of the experiment is to do in-beam γ ray spectroscopy with high energy resolution the best solution would be to choose a semiconductor detector (i.e: germanium detectors) and use a pulser to follow the possible changes in the energy calibration caused by radiation damage during the experiment. In this case we are giving more importance to the energy resolution than to the total detection efficiency. To maintain a good energy resolution is important to reduce the Doppler broadening effect within the intrinsic resolution of the detector. In order to preserve the total detection efficiency, a good solution is to use smaller detectors (in this way we reduce the angular uncertainties at the origin of the Doppler broadening) covering a wide solid angle in the forward direction. To recover the photo-fraction lost with the size reduction we can use the Add-back procedure. As we have seen

in section 4.3, a set of virtually divided Super Segmented Clover Detectors can be a good election in this case.

In an experiment where the most important requirement is to obtain the highest total detection efficiency (if we need i.e. the events in the photo-peak to serve as triggers for a different measurement), and the Doppler broadening effect results a secondary magnitude, the normal procedure would be to choose a detector covering a big solid angle in the forward direction (wide disponibility in different sizes and shapes) in order to have a very high geometric efficiency with an acceptable price. With respect to the other component of the total detection efficiency (the intrinsic efficiency), the best option is a high Z, high density material to increase the photo-fraction. At the same time the material is chosen with an intermediate intrinsic energy resolution, and the Doppler broadening effect tends to be minimized. The CsI Array Detector presented in section 4.3 (with its high geometric efficiency around 47 % for radioactive sources at rest and 84 % for moving sources of $\beta=0.8667c$) is convenient here.

The big gain in total efficiency (almost an order of magnitude) of the CsI array compared with the NaI we use in the last experiment opens new experimental perspectives. In particular , it would be a very interesting solution to study from the systematics of the neutron-rich F isotopes the existence of a new closed shell near the neutron drip-line (limit of nuclear stability) around neutron number N=16 as has been proposed by our group for a future experiment at the FRS.

Bibliography

[1] ENSDF, Table of isotopes

[2] H. Morinaga and T. Yamazaki, In-beam Gamma-ray Spectroscopy (1976) North-Holland Publishing Company.

[3] Radioactive Nuclear Beam Facilities. NUPECC report, April 2000.

[4] R. Grywacz et al., Phys. Rev. Lett. 81 (1998) 776.

[5] T. Motobayashi et al., Phys. Lett. B. 346 (1995) 9.

[6] T. Aumann et al., Phys. Rev. Lett. 84 (2000) 35.

[7] P.G. Thirolf et al., Phys. Lett. B. 485 (2000) 16.

[8] H. Geissel et al., Nucl. Inst. and Methods B 70 (1992) 286.

[9] Marjorie Belleguic. Thèse de Doctorat. Univerity Claude Bernard- Lyon I. May 2000.

[10] http://www.gsi.de

[11] T. Baumann, PhD. Thesis, Univ. Giessen, February 1999

[12] T. Baumann et al., Phys. Lett. B. 439 (1998) 256

[13] M. Smedberg et al., Phys. Lett. B. 452 (1999) 1

[14] A. Navin et al., Phys. Rev. Lett. 81 (1998) 5089

[15] N.M. Magdalena et al., MSUCL-117 (preprint), August 2000

[16] S. Wan, PhD. Thesis, Univ. Heidelberg, May 1999

[17] R. Holzmann et al., GSI Annual Report 1992. pag. 48

[18] V. Hlinka et al., NIM A 419 (1998)503

[19] M. Pfuetzner et al., Nucl. Inst. and Methods B 70 (1994) 213-218.

[20] W.R. Leo, Techniques for Nuclear and Particle Physics Experiments (1993) 157-213.

[21] http://wwwinfo.cern.ch/asdoc/geant_html3/geantall.html

[22] J. Kantele, Handbook of Nuclear Spectrometry (1995) Academic Press

[23] S. Wan et al., Eur. Phys. J.A. (1999) 167

[24] G.G. Kelly, P.R. Bell, R.C. Davis and N.H. Lazar, I.R.E. Trans. Nucl. Sci. Vol. NS-3, No.4 (1956) 57.

[25] HARSHAW/QS scintillation detector catalog.

[26] G. F. Knoll radiation detection and measurement (1989) John Willey and Sons.

[27] http://www-gsi-vms.gsi.de/eb/html/eb_seg_clover.html

[28] T. Lange . Diploma Arbeit. Frankfurt University 2001.

[29] T. Aumann el al. S233 experiment (SIS-LAND_ALADIN).